Modeling of Thin Film Solar Cell Incorporating Space Charge Effects

Mohammad Abdul Mannan

A Thesis

In the Department

of

Electrical and Computer Engineering

Presented in Partial Fulfillment of the Requirements

for the Degree of Master of Applied Science (Electrical Engineering) at

Concordia University

Montréal Québec Canada

August 2011

CONCORDIA UNIVERSITY

School of Graduate Studies

This is to certify that the thesis prepared

By: Mohammad Abdul Mannan

Entitled: Modeling of Thin-Film Solar cells Incorporating Space Charge Effects

and submitted in partial fulfillment of the requirements for the degree of

Master of Applied Science (Electrical Engineering)

complies with the regulations of the University and meets the accepted standards with respect to originality and quality.

Signed by the final examining committee:

_____ Chair
Dr. Rabin Raut

_____ Examiner
Dr. Mojtaba Kahrizi

_____ Examiner
Dr. A. K. Waizuddin Ahmed

_____ Supervisor
Dr. M. Z. Kabir

Approved by _____
Dr. W. E. Lynch
Chair , Department of Electrical and Computer Engineering

_____2011 _____
Dr. Robin A. L. Drew
Dean, Faculty of Engineering and Computer Science

ABSTRACT

Modeling of Thin-Film Solar Cells Incorporating Space Charge Effects

Mohammad Abdul Mannan

Due to scarcity of fossil fuel and global warming issue photovoltaic conversion of sunlight into electricity is the most reliable one to mitigate the huge future energy demand. Substantially cost reduction of solar cell technology is urgently needed for expanding the solar cell technology in grid system. To achieve this goal polycrystalline CdTe based thin film solar cell is in the focus of researchers for the last decades and extensive work and improvement has been done on this area.

A suitable model is needed to describe current-voltage (J-V) characteristics, properly understanding the operating principles of a thin-film solar cell and optimizing its overall efficiency. Until now, few models were proposed in the literature however those models are either oversimplified or having too many fitting parameters. In all previous models it is assumed that electric field throughout the devices is uniform. However practically the electric field is not uniform and varies along with absorber layer due to space charge. The variation becomes more significant with the increase of space charge density and the electric field collapses somewhere in the absorber layer when space charge density crosses a limit. In polycrystalline material presence of crystallographic defects (such as dislocations, vacancies, interstitial, dangling bonds, distorted bond angles) in the grain boundaries lead to the formation of electronic states.

These electronic states act as a trap centers for carriers. Due to these trapped carriers electric field in the absorber layer is no more uniform.

This work is aimed at developing a model to describe J/V characteristics of major thin-film photovoltaic (PV) which currently are CdTe based and $CuIn(Ga)Se_2$ based materials. We emphasize the properties which are realistic to these types of PV and are not adequately reflected in the existing models. They are: (1) non uniform electric field, (2) exponential photon absorption, (3) actual solar spectrum, (4) uniform and exponential distribution of space or trapped charge density, (5) collapse of Electric field and depleted region is less than the absorber layer width and (6) the effect of diffusion current.

A model for the external voltage dependent photocurrent is determined by solving the continuity equation for both electrons and holes. The overall load current is calculated considering the actual solar spectrum. The model is fitted with the published experimental data and shows a very good agreement.

To my loving parents

&

My wife and daughter

ACKNOWLEDGMENTS

Foremost, I would like to thank my wife Farhana Anjum for her inspiration, support to complete the master's degree and especially for her patience during this endeavor. I am indebted to Dr. M. Zahangir Kabir for his continuous guidance, encouragement, help and financial support during this research work. I also would like to extend my deepest gratitude to my parents, brothers and sisters for giving me encouragement, support throughout my life. This work would not be possible without the warm, healthy and knowledgeable discussion with all the members of our research group. I am grateful to my colleagues Mr Mazharul Huq Chowdhury , Mr. Md Shahnawaz Anjan and Mr. Shaikh Asif Mahmood for their useful discussions. I also would like to show my gratitude to the professors and staffs at Concordia University. Many thanks go to Dr. Irina Stateikina, Dr. Pouya Valizadeh and Dr. Pragasen Pillay for their encouragement during the course of my Master's program. Finally, I am gratefully to our creator almighty ALLAH.

TABLE OF CONTENTS

LIST OF FIGURES

LIST OF TABLES

LIST OF ABBREVIATIONS

PV	-	Photo Voltaic
Cd	-	Cadmium
Pb	-	Lead
Se	-	Selenium
a-Si	-	amorphous silicon
FF	-	Fill Factor
CdTe	-	Cadmium Telluride
CdS	-	Cadmium Sulfide
Cu_2S	-	Copper Sulfide
$CuInSe_2$	-	Copper Indium Selenide
CIGS	-	Copper Indium Gallium Selenide
AM	-	Air Mass
CIS	-	Copper Indium Selenide
ZnTe	-	Zink Telluride
ITO	-	Indium Tin Oxide
I_O	-	Incident Photon flux
$Cu(InGa)Se_2$	-	Copper Indium Gallium Selenide

CHAPTER 1 INTRODUCTION

1.1 Sun Energy

Sun provides colossal amounts of energy powering atmospheric currents, oceans, and evaporation cycle, river flow, hurricanes and tornadoes that demolish natural landscape. Humans annually use about 4.6×10^{20} joules, which sun supplies in one hour. The sun continuously supplies about 1.2×10^{5} terawatts of energy which is very much greater than any other renewable or non renewable sources of energy can provide. This energy is much greater than the energy required by human beings which is about 13 terawatts. 20 Terawatts of energy which is about two times of total fossil fuel consumption of the world can be produced by covering only 0.16% of Earth's land with 10% efficient solar cells [1]. Solar energy is in abundance but only a very little is used to directly power human activities.

1.2 Energy Crisis and Photovoltaic Cell

The demand for energy has always been the primary driving force in the development of industrial capability. The invention of the steam engine sparked the industrial revolution and the consequent evolution of an energy economy based on wood and coal. Since then the continuous growth of the energy economy has focused on various sources of energy, such as nuclear, wind, water, coal, oil and gas. Enormous -increasing demand of energy due to superior living standard overstepping its supply. The world is progressively marching towards a serious energy crisis. With each passing day coal, oil and gas are

moving towards being extinct and electrical energy sources using coal, wood, gas, and oil generate large amount of pollution or carbon dioxide emissions, thereby posing health risk. Nuclear energy is very expensive and poses radiation hazards and nuclear waste problems. All these electrical energy power sources require large capital investments and schedule maintenance. Current oil crisis, high oil price, geopolitical tensions over oil resources and nuclear energy, global warming caused by burning fossil fuels compelled energy planners to look for alternative sources to reduce reliance on fossil fuels.

There is an attention in renewable energy sources such as those derived from wind power, hydro power, or conversion of fast growing crop into ethanol. These are universally available and potentially help to lessen global warming by reducing the carbon footprint. Then, there is a third kind of energy source based on photovoltaic conversion of sunlight into electricity by certain widely available semiconductors, which is possibly the cleanest, most accessible, and potentially the most reliable alternative. A solar energy source provides pollution-free, self-contained, reliable, quite, long-term, maintenance-free, and year-round continuous and unlimited operation and moderate costs.

Photovoltaic energy conversion refers to the direct conversion of the light energy into usable electrical energy which can be consume immediately or stored. Photovoltaic energy conversion in solar cells consists of two essential steps. First, absorption of light generates an electron-hole pair. The electron and hole are then separated by the structure of the device – electron to the negative terminal and holes to the positive terminal-thus generating electrical power.

1.3 Chronological History of Development Solar Cell

Year	Activity
1839	The photovoltaic effect was first discovered by Alexandre-Edmond Becquerel, who was a French physicist.
1876	William Grylls Adams and Richard Evans Day proved that it is possible to convert solar energy into electricity directly.
1883	A description of the first solar cells made from selenium wafer was made by Charles Fritts.
1905	Albert Einstein claimed that light consists of "packets" or quanta of energy, which we now call photons.
1916	Robert Andrews Millikan provided experimental proof of the photoelectric effect.
1923	Albert Einstein received the Nobel Prize for his theories explaining the photoelectric effect
1950s	Bell Labs produce solar cells for space activities.
1953	Dr. Dan Trivich of Wayne State University makes the first theoretical calculations of the efficiencies of various materials of different band-gap widths based on the spectrum of the sun

1954 Three researchers, Gerald Pearson, Daryl Chapin and Calvin Fuller, at Bell Laboratories discovered a silicon solar cell, which was the first material to directly convert enough sunlight into electricity to run electrical devices.

1958 The first PV-powered satellite, Vanguard I, was launched. The solar panel had an area of 100cm² and delivered an effect of approximately 0.1W. The satellite power system operated for 8 years.

1963 A Japanese electronics manufacturer, Sharp Corporation, produces a viable photovoltaic module of silicon solar cells.

1980 At the University of Delaware, the first thin-film solar cell exceeds 10% efficiency. It's made of copper sulfide (Cu_2S) and cadmium sulfide (CdS).

1992 University of South Florida develops a 15.9% efficient thin-film photovoltaic cell made of cadmium telluride, breaking the 15% barrier for the first time for this technology.

1994 The National Renewable Energy Laboratory develops a solar cell, made from gallium indium phosphide and gallium arsenide that becomes the first one to exceed 30% conversion efficiency.

1999 The National Renewable Energy Laboratory achieves a new efficiency record for thin-film photovoltaic solar cells. The new measurement is of 18.8 percent efficiency.

2007 The university of Delaware achieved a 42.8% solar cell efficiency

1.4 Advantages and Disadvantages of Solar cell Technology

The advantages and disadvantages of solar cell technology are described in the following table [2]

Table 1-1: Advantages and disadvantages of solar cell technology

Advantages of solar cell technology	Disadvantage of solar cell technology
▪ Fuel source is vast and essentially infinite ▪ No emissions, no combustion or radioactive fuel for disposal (does not contribute to global climate change or pollution) ▪ Low operating cost (no fuel) ▪ No Moving Parts (no wear) ▪ Ambient temperature operation (no high temperature corrosion or safety issue) ▪ High reliability in module (> 20 years) ▪ Modular (small or large increments) ▪ Quick installation ▪ Can be integrated into new or existing building structures ▪ Can be installed at nearby any point of use. ▪ Daily output peak may be match local demand ▪ High public acceptance ▪ Excellent safety record	▪ Fuel source is diffuse (sunlight is relatively a low density of energy) ▪ High installation cost ▪ Power reliability auxiliary (balance of system) elements including storage ▪ Lack of widespread commercially available system integration and installation so far ▪ Lack of economical efficient energy storage

1.5 Market of Solar Cell

The high cost of power from solar photovoltaic (PV) panels has been a major deterrent to the technology's market penetration. Due to technological developments, more efficient production and large scale production, the costs of solar panels would fall significantly. The average price for a PV module, excluding installation and other system costs, has dropped from almost $100 per watt in 1975 to about $4 per watt at the end of 2007 as shown in Figure 1-1[3].

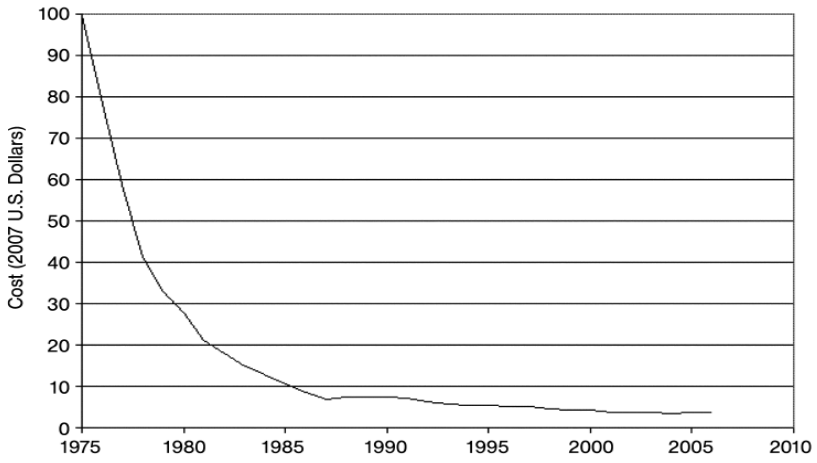

Figure 1-1: Average cost per watt of PV module 1975-2006 [3].

In 2004, a prediction of an industry's practitioner concluded that for "thin film PV alone, production cost are expected to reach $1 per watt in 2010" [4], a cost that makes solar PV competitive with coal-fired electricity. Figure 1-2 compares cost projection of solar electricity with that produced by conventional sources [5]. In 2009, the average cost of grid –supplied electricity in the United States was 9.5 ¢/kWh, and this value will continue to rise due to rise of fossil fuel price. The current price of electricity generated using solar

cell remains two or three times greater than grid supplied electricity, but PV costs continue to decrease. A crossover, commonly known as "grid parity" is expected sometime during the next decade.

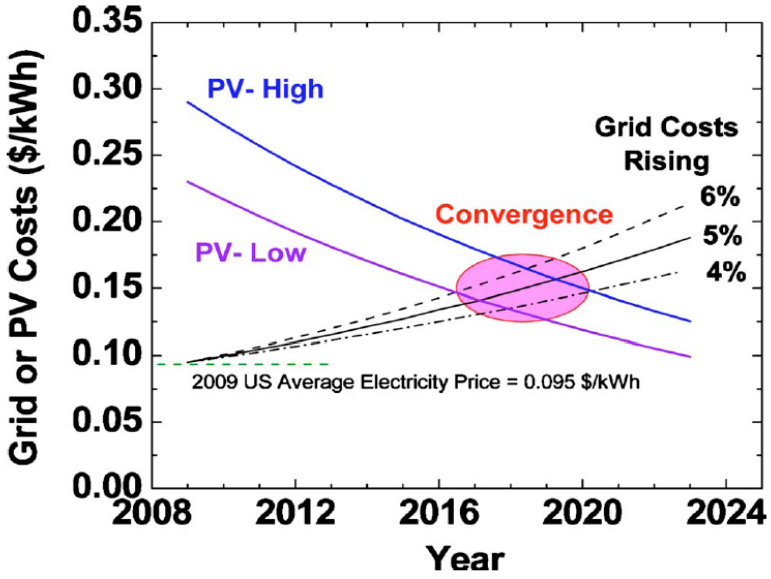

Figure 1-2: Projected convergence of the cost of electricity produced by PV and the conventional grid prices [5]

The market for solar panels in the world has been growing at an average rate of >40%/year over the past decade [5]. In 2009 the installed photovoltaic power exceeded 8GW. In 2010 a staggering 15GW of solar power was installed [6]. Experts expect that production of solar panels will be 14 times as big over ten years compared to current outputs. According to European Renewable Energy Commission (EREC) in 2040 renewable energy source will cover 29.808 TWh out of total 36.346 TWh world electricity consumption, a largely dominant portion of renewable energy will be covered

by PV module. The relative contribution of different sources to total renewable energy production in 2040 is shown in Figure1-3 [7].

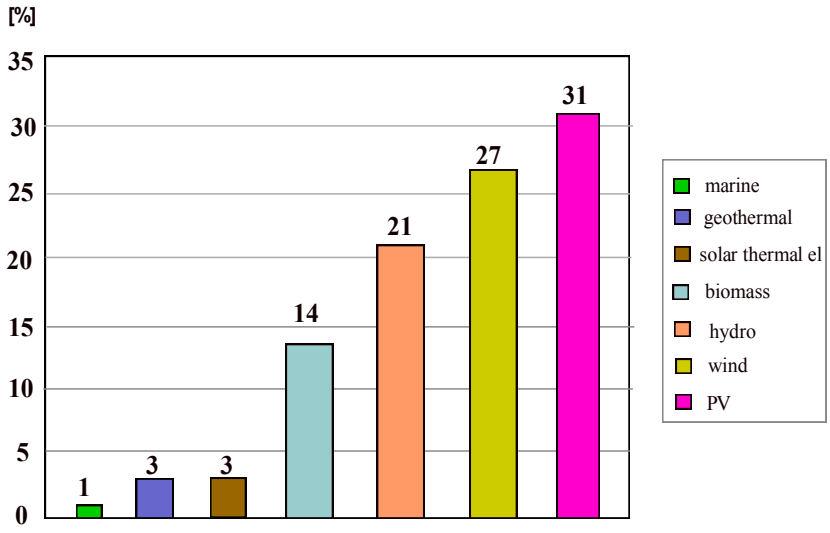

Figure 1-3: Prediction scenario by 2040; contribution of different energy sources to total electricity consumptions of 36.346 TWh[7].

1.6 Application of Solar Power Systems

Since PV energy systems provide a fuel-free , pollution-free, and uninterrupted source of electricity , solar energy systems are suited for many applications, such as landing obstruction lights for airport, water pumping for irrigation, power sources for homes and commercial buildings, perimeter alarm transmitters, electronic border fences, intrusion alarms for security , highway signs, portable backpack radios, remotely located, unnamed electronic surveillance systems, educational TV broadcasting , railroads, radio relay stations, navigation aid sensors, ocean based earthquake systems, emergency alarm

transmitters, communication satellites and space –based missile surveillance and reconnaissance systems.

1.7 Research Motivation

Research shows that the cost of second-generation thin-film polycrystalline solar cell is lower compared to the single crystal solar cells [8]. In addition the thin-film solar cells use lesser amount of raw materials and thus lighter compared to the crystalline cells. The second-generation thin film solar cells are increasingly promising for their cheaper production and better efficiency. Cells based on (i) polycrystalline CdTe, (ii) polycrystalline $CuIn_{1-x}$ Ga_xSe_2 (CIGS) and (iii) hydrogenated amorphous Si (a-Si:H) absorbers are the three most potential photoconductors for thin film solar cells because of their excellent efficiency [9]. The subscript x represents the mole fraction. The CdTe and CIGS based cells are p–n heterojunction cells, and incident photons are mainly absorbed in the p-layer and the photo carriers are collected by the built-in electric field in this layer. The a-Si:H solar cells use p-i-n type structure where the incident photons are mainly absorbed in the i-layer in a-Si:H solar cells. The voltage dependent charge collection in the depleted absorber layer is the dominant charge collection mechanisms in thin film solar cells [10,11].

There has been an active theoretical and experimental research to improve the performance of these devices. The textbook of Wagemann and Eschrich [12] gives a closed-form expression for the dark *J/V* equation, but this expression holds only for

voltages around the point $V = 0$. Misiakos [13] proposed two different models for strong and uniform absorbed light and in both models it is needed to define a limiting carrier. Crandall [14] derived a model for a-Si solar cells which holds only for some of the *J/V* characteristics because the underlying model neglects diffusion currents. Taretto et al. [15] presents a model for the J/V equation in pin diodes and pin solar cells. Taretto model is valid only below a critical current density J_{CR} and it assumed that photo generation rate is homogeneous throughout the solar cell. Hegedus et al. reviewed a few theoretical models to describe the current–voltage (J–V) characteristics in thin film solar cells [16]. They have shown that the most successful model calculates the photocurrent by considering carrier drift and utilizing Hecht collection efficiency formula in the nearly intrinsic absorber layer. However, this models has made an unrealistic assumption that all the carriers are generated at the top interface of the absorber layer for all incident photon and used a number of fitting parameters such as maximum photocurrent with complete charge collection, reverse saturation current, effective attenuation coefficient, series resistance and carrier ranges.

All of the above discussed models assumed electric field distribution in the depletion layer is uniform. However electric field distribution is non uniform in all practical devices and this non uniformity depend on space and trapped charge density. The electric field becomes more non uniform with increase of space and trapping charge density and collapses in somewhere of the absorber layer when space or trapped charge density exceed a limit. Therefore it is necessary to develop a model to describe the J/V

characteristics of solar cell in non uniform electric field considering an arbitrary amount of space and trapping charge density.

1.8 Research Objective

In thin film solar cell electric field distribution is changed due to space or trapped charges. The electric field collapses when space charge density exceeds a limit and electric field do not exist throughout the absorber layer results in a reduction of drift region. Electric field distribution depends upon the space charges density, the total device thickness and the built-in voltage. The overall objectives of this research work are,

(i) To develop a model for J/V characteristics of thin film solar cell under actual solar spectrum considering the space charge effects on electric field profile.

(ii) To analyze the carrier transport when electric field collapse somewhere in the middle of device length.

(iii) To analyze the effect of space charge density , carrier transport properties, surface recombination velocity, temperature, series resistance , device width and window layer thickness on J/V characteristics of thin film solar cell

(iv) To verify the model with the published experimental data on CdTe, CIGS.

This model has been developed based on $n^{+}p$ structured thin film solar cell and the model is applied to CdS/CdTe and CIGS thin film solar cells. However the same model can be used to analyze the J/V characteristics of thin film solar cell made of other photovoltaic material and other polycrystalline photoconductive materials (e.g., poly-CdZnTe, poly-PbI_2) by changing the model parameters according to the photoconductive material. The

model can also be used to describe the detector response to exposure of polycrystalline (HgI_2 , CdZnTe, poly-PbI2) X-ray detector.

1.9 Research Outline

The thesis is divided into five chapters. Following this introductory chapter, few basic theories and important terminologies are discussed in chapter two. The proposed model and the formulation of *J/V* equation considering non uniform electric field distribution, exponential photon absorption, carrier trapping, carrier drift and diffusion are discussed in chapter three. Chapter 4 presents results and discussions. Finally, Conclusions, contributions and future work are summarized in chapter five.

CHAPTER 2 : BACKGROUND THEORY

2.1 Semiconductor p-n Junction

When an n-type semiconductor and a p-type semiconductor are joined, a p-n junction device is formed. If the materials in the p-type and the n-type regions are the same, the junction is called homojunction, but when the materials in the p-type and the n type regions are different, the junction is called heterojunction. Figure 2-1 shows the schematic of a p-n junction.

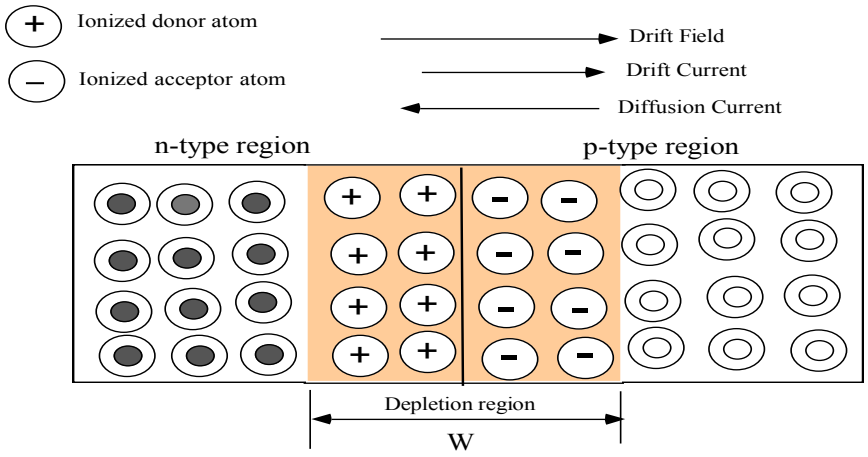

Figure 2-1: The schematic and the band diagram of a p-n junction

Due to the gradient of the carrier density, majority-carrier electrons diffuse from the n-type region to the p-type region, and majority-carrier holes diffuse from the p-type region to the n-type region. This carrier diffusion will produce a diffusion current flow from the

p-type region to the n-type region. The charged dopants will create a built-in potential and can be expressed as

$$V_{bi} = \frac{kT}{q} \ln\left(\frac{N_A N_D}{n_i^2}\right) \tag{2.1}$$

Where, k is Boltzmann's constant, T is absolute temperature, q is charge of an electron, N_A is the acceptor concentration , N_D is donor concentration and n_i is intrinsic carrier concentration.

This build-in field will produce a drift current opposite direction to the diffusion current. In thermal equilibrium drift and diffusion current are equal and the Fermi energy levels in the p-type region and n-type region are aligned to coincide and an electrostatic potential difference exists across the depletion region. Figure 2-2 shows the energy band diagram for p-n junction under equilibrium.

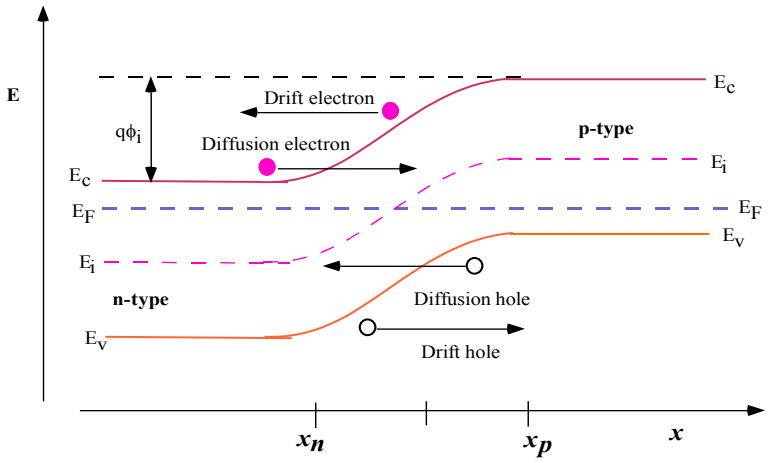

Figure 2-2: Energy Band Diagram of a p-n Junction in Thermal Equilibrium, carrier flow and current direction

2.2 Working of p-n Junction as PV Cell

The term photovoltaic is derived by combining the Greek word for light, photons, with voltaic, named after Alessandro Volta. A photovoltaic (PV) cell converts sunlight to electricity. In solar cell the internal built-in potential of p-n junction drives photo generated electrons and holes to the opposite terminal as shown in Figure 2-3.

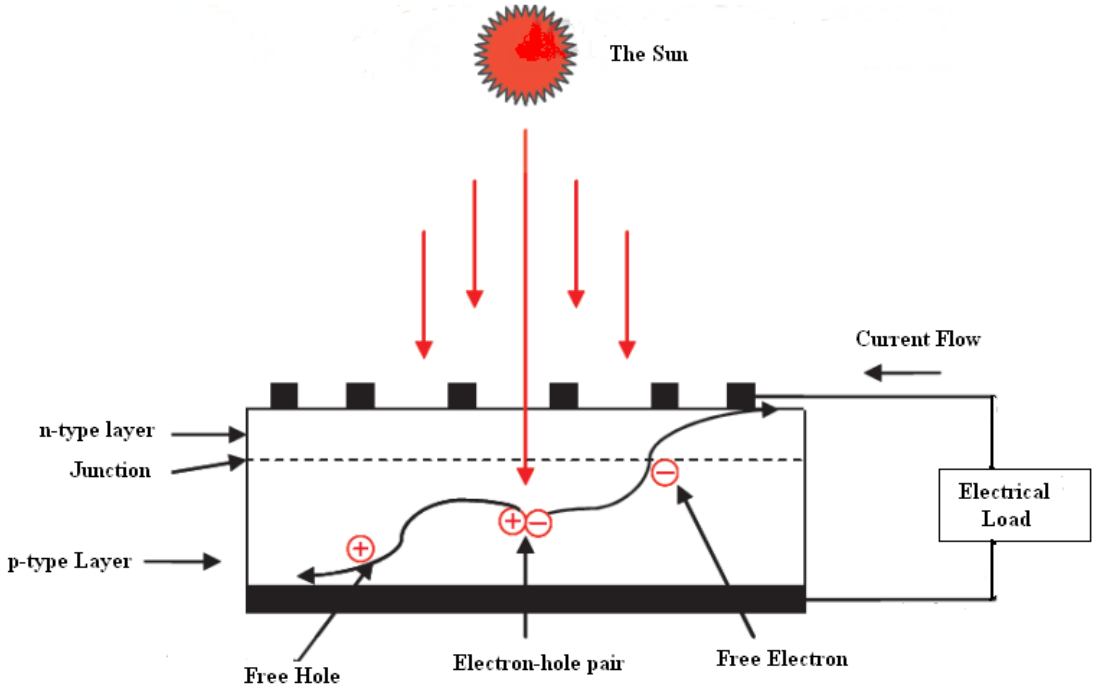

Figure 2-3: An illustration of the operation of a p-n junction solar cell showing the generation and movements of free carriers

Solar Cell works like a semiconducting diode, which is optimized in order to get maximum electrical power when exposed to sunlight. When a photon strikes the cell, it is absorbed by an electron in the valence band and therefore provides energy to the electron elevating it to the electronic state in the conduction band leaving a hole in the

valence band. These electrons and holes act as free charge carriers and contribute to the current. In the absence of the electric field both electron and hole randomly move until they recombine. If during this random movement they get into the space charge region of the p-n junction they are separated by the electric field as shown in Figure 2-4.

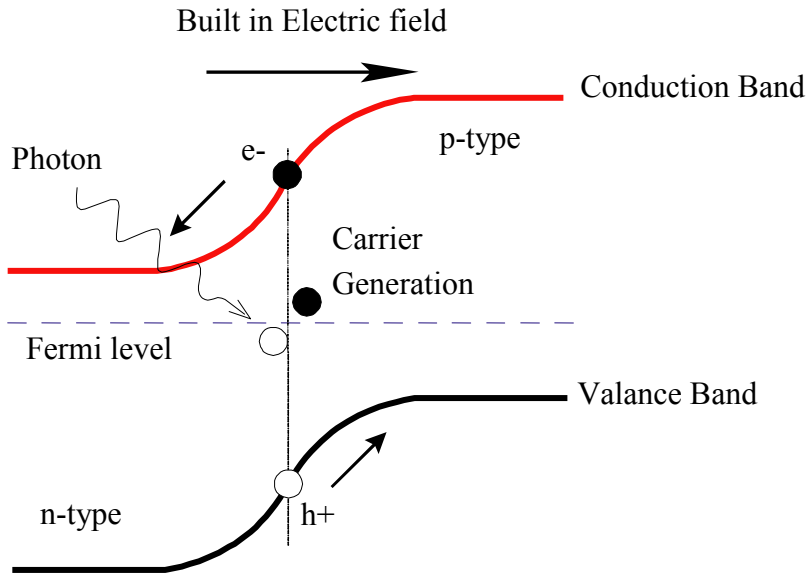

Figure 2-4: Light absorption, a photon generates an electron- hole pair and are separated over the junction and collected by a circuit and can then run an external load

A conventional solar cell consists of two layers of semiconductor, one positive (p-type) and the other negative (n-type), sandwiched together to form a p/n junction as shown in Figure 2-5.

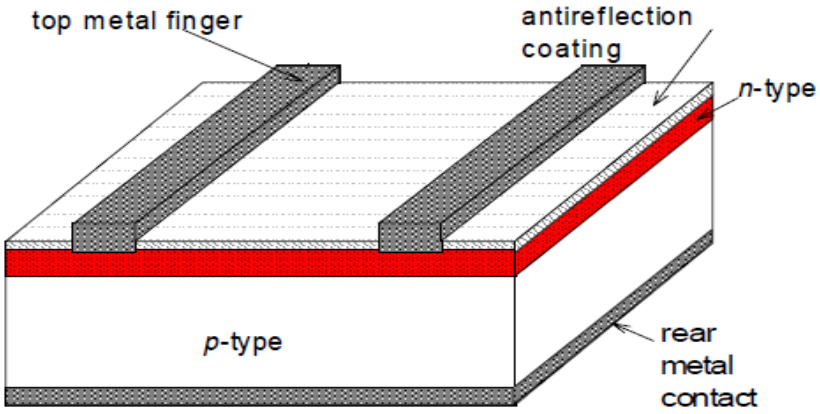

Figure 2-5: Structure of conventional Solar cell

2.3 Carrier Generation by Optical Absorption

The principle means of carrier generation in solar cell is the absorption of light. For a planar slab as shown in Figure 2-6, a photons which enters the semiconductor generates $g(x)\delta(x)$ electron hole pair in a thin layer at depth $x \to x+\delta(x)$

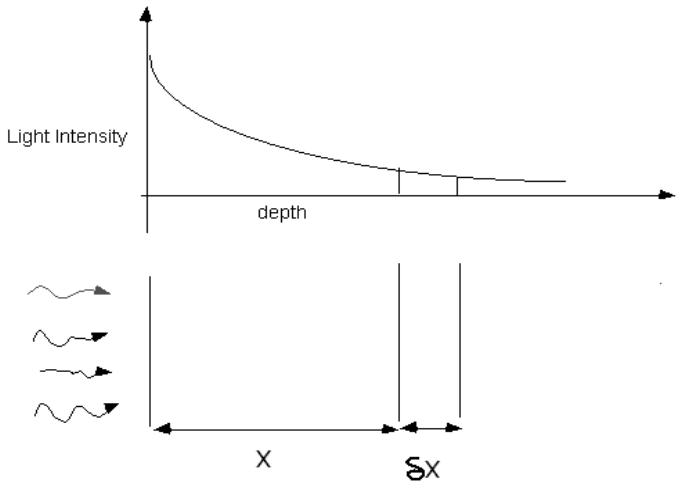

Figure 2-6: Light absorption in semiconductor

The carrier generation function is given by

$$g(x) = \alpha(x)\exp\{-\alpha(\lambda)x\} \qquad (2.2)$$

where α (λ) is the absorption co-efficient. Figure 2-7 [17], shows the absorption co-efficient of semiconductor commonly used in photovoltaic applications.

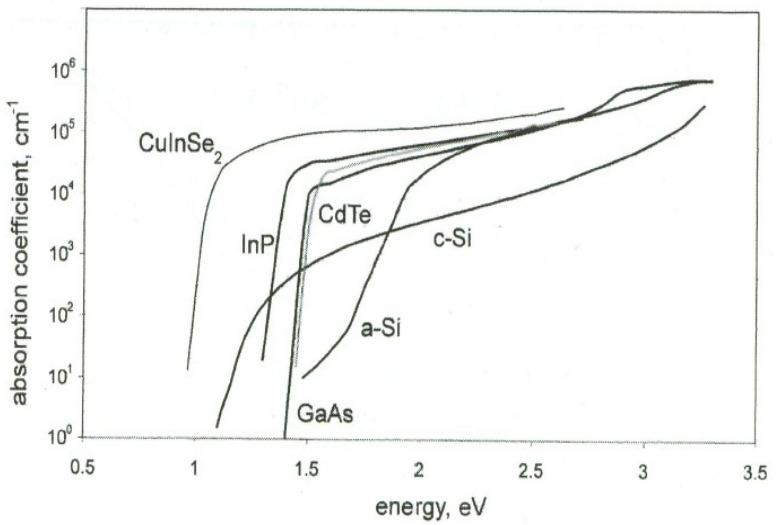

Figure 2-7: The absorption coefficients of the principle semiconductors used in solar cell manufacture [17].

2.4 Carrier Recombination

Recombination is result in annihilation of free electron-hole pairs. Recombination is mainly classified as bulk and surface recombination.

2.4.1 Bulk Recombination Process

The most frequent encountered recombination in practical operation of solar cells is radiative, Auger and defect-assisted recombination process [18] .These processes are depicted schematically in Figure 2-8.

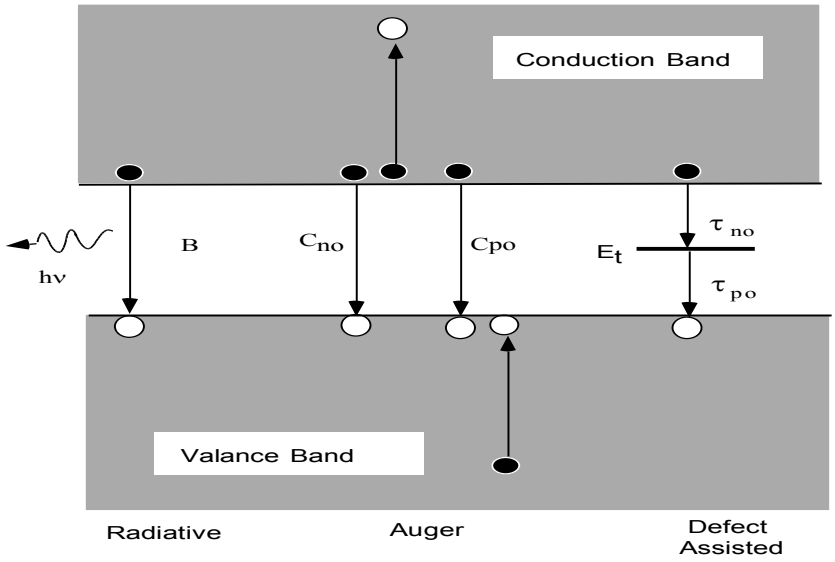

Figure 2-8: A schematic diagram of the principal recombination processes in semiconductors, the direction arrows indicates electron transition.

The rate of band to band radiative recombination can be written in the form

$$U_{rad} = B\left(np - n_i^2\right) \tag{2.3}$$

Where, B is radiative recombination co-efficient, n is electron concentration, p is hole concentration and n_i is intrinsic carrier concentration.

The rate of band to band Auger recombination can be written as

$$U_{Auger} = \left(C_{po}p + C_{no}n\right)\left(np - n_i^2\right) \tag{2.4}$$

Where, the C_{p0} and C_{n0} are Auger terms.

The recombination rate via defects of concentration N_t with a level at energy E_t within the band within the band gap is described by the Shockley-Read-Hall formula [19]

$$U_{SHR} = \frac{np - n_i^2}{\tau_p\left(n + n_1\right) + \tau_n\left(p + p_1\right)} \tag{2.5}$$

Where, $n_1 = n_i \exp\left(\frac{E_t - E_i}{k_B T}\right)$, and $p_1 = p_i \exp\left(\frac{E_t - E_i}{k_B T}\right)$

Where, k_B is the Boltzmann constant, τ_n , τ_p are parameters, proportional to the defect concentration N_t, which are characteristics for the particular defect and energy level. At low injection, $\tau_{n,\text{ and }}$ τ_p are assumed as the minority carrier lifetimes.

2.4.2 Surface Recombination Process

Surface recombination velocity is an important parameter which affects the dark saturation current and the quantum efficiency of solar cells. Similar to dislocations and planar defects such as grain boundaries, surfaces introduce band of electronic states in the band gap which can be ascribed to broken (or strained) and impurities. A complete characterization of surface recombination must also be taken into account the surface charge which may give rise to band bending. To achieve optimal operation, surface

recombination is reduced by passivating or integrating window layer which prevents minority carriers from reaching the surface. Under identical process parameters the dependence of the surface recombination velocity on the surface doping concentration can be identified. Cuevas et al. proposed the following analytical relationship between surface recombination velocity and doping concentration for an oxidized silicon surface [20] :

$S = 70 cm/s$ for $N < 7\times10^{17} cm^{-3}$

$$S = 70\left(\frac{N}{7\times10^{17}}\right) \text{ for } N > 7\times10^{17} cm^{-3}$$

2.5 Solar Cell Parameters

An ideal solar cell can be represented by a current source connected in parallel with rectifying diode as shown in Figure 2-9.

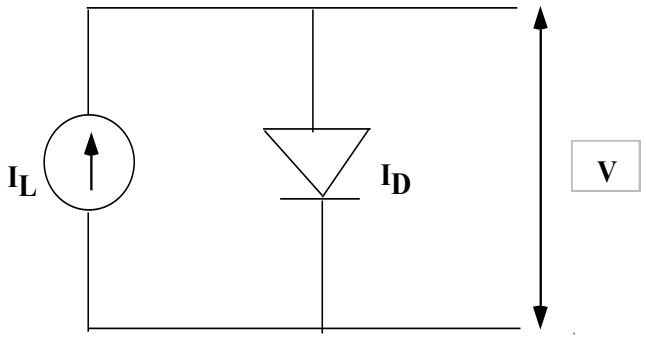

Figure 2-9: Circuit model of an Ideal Solar cell, a current source parallel with rectifying diode

The corresponding I-V characteristics is described by the Shockley solar cell equation

$$I = I_{ph} - I_0 \left[\exp(\frac{qV}{K_B T}) - 1 \right] \quad (2.6)$$

Where K_B is the Boltzmann constant, T is the absolute temperature, q is the electron charge, and V is the voltage at the terminals of the cell. I_0 is diode reverse saturation current. The photodiode current I_{ph} is related to the photon flux incident on the cell and the external voltage.

2.5.1 Short Circuit Current, I_{sc}

Figure 2-10 (a) shows a typical Current-Voltage (I-V) characteristics curve. In ideal case short circuit current I_{SC} is equal to the photo generated current I_{ph}. P_m is the point on I-V curve where output power will maximum. Figure 2-10 (b) shows how the output power of a solar cell varies with output voltage.

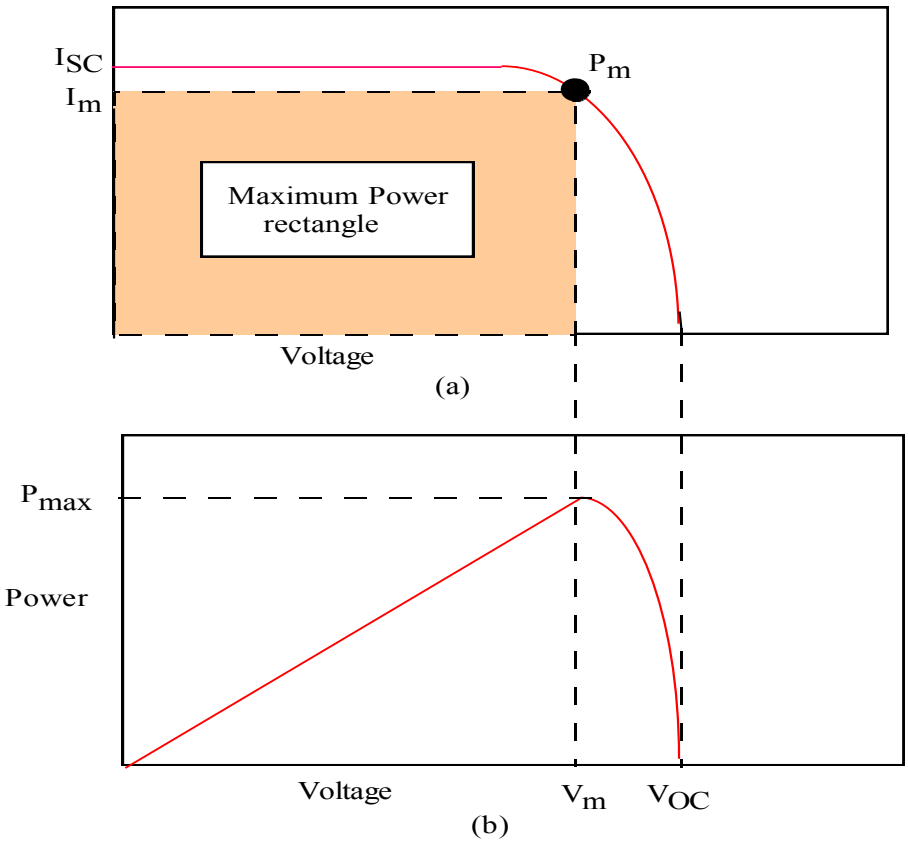

Figure 2-10: (a) The I-V Characteristics of an ideal solar cell, (b) the power produced by the cell. The power generated at the maximum power point is equal to the shaded rectangle.

2.5.2 Open Circuit Voltage, V_{OC}

The voltage developed when terminals are open (Infinite load resistance) is called open circuit voltage, V_{OC} is given by

$$V_{OC} = A\left(\frac{K_B T}{q}\right)\ln\left(1+\frac{I_{ph}}{I_0}\right) \tag{2.7}$$

Where A is diode ideality factor, K_B is Boltzmann's constant, T is absolute temperature, q is electron charge, I_{ph} is voltage dependent photo current, I_0 reverse saturation current.

2.5.3 Power

The Power P = IV produced by the cell is shown in Figure 2-10 (b). The cell generated the maximum power P_m at a output voltage V_m and current I_m .

$$P_{\mathrm{m}} = V_m I_m \tag{2.8}$$

The maximum power point can easily determined from voltage-current characteristics of solar cell. At any output voltage less or greater than V_m , the output power will be less than P_m.

2.5.4 Fill Factor, *FF*

Fill Factor FF is a figure of merit of the solar cell and defined as the ratio of the maximum power to the product of Voc and Isc.

$$FF = \frac{V_m I_{\mathrm{m}}}{V_{OC} I_{SC}} \tag{2.9}$$

The J-V characteristic of an ideal solar cell complies with the superposition principle as shown in Figure 2-11. The dependency of solar cell current to voltage can be obtained from the corresponding characteristic of a diode in the dark by shifting the diode characteristic along the current axis by I_{ph}. However the J-V characteristics curve deviates from the ideal curves due to various losses.

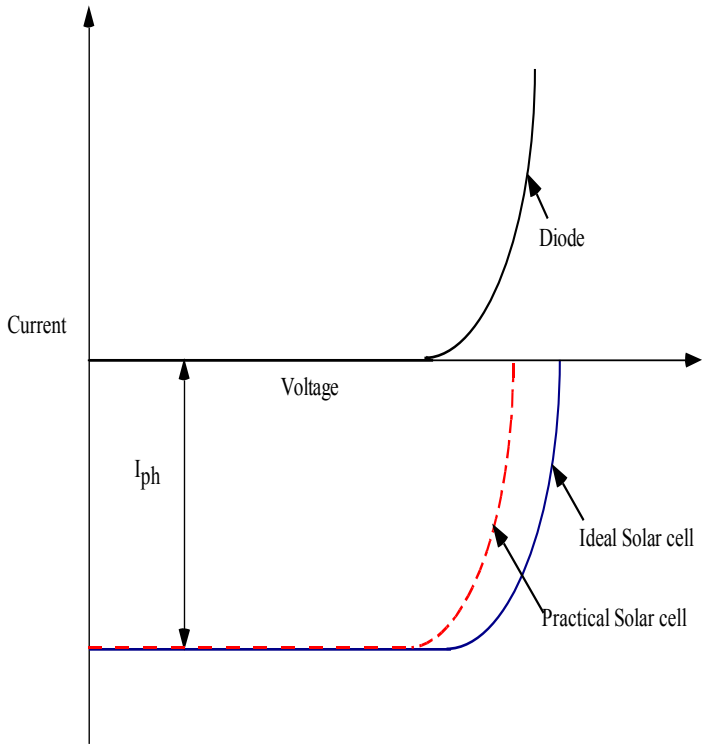

Figure 2-11: J-V curves for diode, ideal and practical solar cell. The difference between the ideal and practical solar cell is attributed to losses

2.5.5 Efficiency, η

The efficiency of the solar cell is defined as the ratio of electrically generated power P_{out}, to the input power P_{in}, on the cell.

$$\eta = \frac{P_{out}}{P_{in}} = \frac{V_{OC} I_{SC} FF}{P_{in}} \tag{2.10}$$

2.5.6 Series and Shunt Resistance

The losses in the solar cell can be represented by adding a series and shunt resistance to the ideal solar cell structure as shown in Figure 2-12.

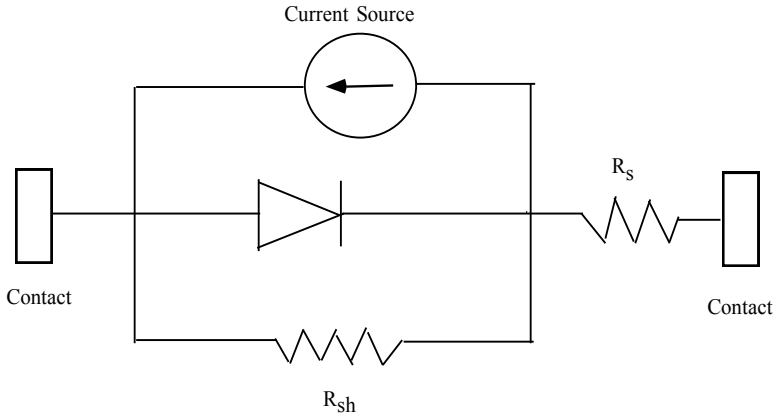

Figure 2-12: Circuit Model for a practical solar cell, considering the effects of series and shunt resistance

Series Resistance: The series resistance of a solar cell is mainly due to metal-semiconductor contact resistance, ohmic resistance in metal contacts, and ohmic resistance in semiconductor substrate. The R_s is the resistance the carriers find on their way, it is due to the low conductivity of the window layer and absorber layer and recombination of carriers into the bulk materials. The series resistance reduces the maximum achievable output power and hence softens the I–V characteristics of a solar cell in the fourth quadrant, eventually degrading fill factor of the solar cell. It is found that the fill factor of a solar cell decreases by about 2.5% for each 0.1 ohm increase in series resistance [21]. In open-circuit condition the current is zero and the voltage drop

across the R_S is also zero, so the V_{oc} is not affected by the R_S. For small value of series resistance short circuit is not changed. However when series resistance is sufficiently large, it limits the short circuit current. Variation in I-V characteristic due to change in R_s is shown in Figure 2-13.

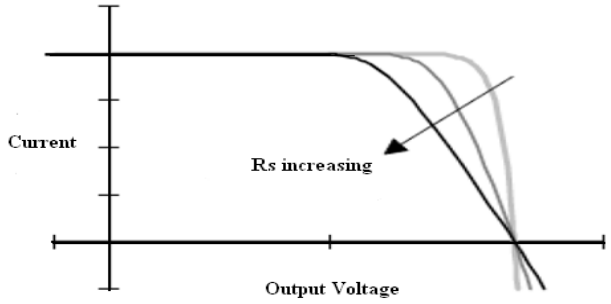

Figure 2-13: Effect of Series resistance on the I-V curve of a Solar cell

Shunt Resistance: A fraction of the photo generated carriers can flow through the surface of the devices instead of flowing through the external load. These effects that prevent photo generated carriers from following in the external circuit can be represented by an effective internal shunt or parallel resistance that diverts the photocurrent away from the load. The Shunt resistance degrades the fill factor and V_{oc}. If the resistance of the diode is more than the R_{sh}, it enables current path through the shunt resistance thereby affecting the V_{oc}. Variation in I-V characteristics with R_{sh} is shown in Figure 2-14.

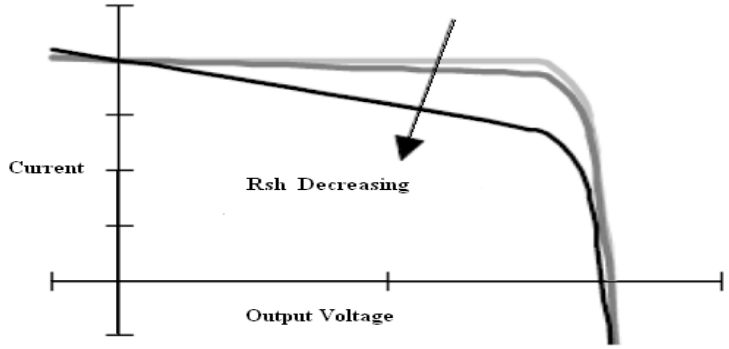

Figure 2-14: Effect of shunt resistance on the I-V curve of a Solar cell

2.6 PV Materials

PV cells are made of semiconductor materials with crystalline structure and thin film materials with poly crystalline structure. The majority of PV-cells are silicon-based , however in the near future poly crystalline thin film materials are likely going to surpass silicon PV cells in terms of cost and performance [22]. PV materials may fall into one or more of the following classes: crystalline, thin film, amorphous, multi-junction, organic or photochemical.

2.6.1 Crystalline Materials

A first reasonably efficient solar cell was possible in 1954 by the rapid development of crystalline silicon technology for miniaturized electronics. Since then the majority of solar cells fabrication have been based on silicon in mono crystalline or polycrystalline form.

Single-crystal silicon: Mono-crystalline silicon cells have in the past dominated the PV market but have now been overtaken by poly-crystalline silicon. The popularity of mono-crystalline silicon was due to the high efficiency, good stability and desirable electronic, physical and chemical properties of silicon. Moreover, silicon was already successful in microelectronics and the enormous industry thus created would benefit the smaller PV industry with regards to economy of scale [23].

Poly-crystalline silicon: This is the currently most dominant material and has surpassed the mono-crystalline because it is cheaper. The cost of silicon is a significant portion of the cost of the solar cell. The manufacturing process of poly-crystalline silicon reduces the cost of silicon by avoiding pulling in the manufacturing process and it results in a block with a large crystal grain structure. This results in cheaper cells with a somewhat lower efficiency. The assembly of multi-crystal wafers is easier and therefore offsets the low efficiency disadvantage.

Gallium Arsenide: This material is a compound semiconductor made of gallium and arsenic. It has a crystalline structure and has a high level of light absorption. GaAs has higher efficiency than silicon but its main drawback is its cost. It use mainly in space applications.

2.6.2 Thin-film Materials

Crystalline silicon has been the dominant photovoltaic technology since the development of the first solar cell in the Bell Laboratories. When talking about drawbacks of Si, we can say that Si is the most weakly absorbing semiconductor used for solar cells because it has an indirect bandgap while most of the other semiconductors have a direct bandgap. Therefore, at least ten times more crystalline Si is needed to absorb a given fraction of sunlight compared to other semiconductors like GaAs, CdTe, $Cu(InGa)Se_2$. Thicker semiconductor material means higher material volume and also a higher quality material because of the long paths that the high-energy electrons excited by the photons must travel before they are delivered to the external circuit to produce useful work. All this leads to high material cost.

Since the 1990s development of thin-film, processes for manufacturing solar cells have increased significantly [24]. These PV devices are made using very thin semiconductor films deposited on some type of low-cost structural substrate such as glass, metal or plastic as shown in Figure 2-15. Epitaxial processes (such as vapor deposition, sputter processes and electrolytic baths) are used to achieve this. Because of high absorption coefficient the deposited layer of PV material is extremely thin. This results in the reduction of the dominating material cost although thin-film PV cells suffer from poor cell conversion efficiency. There are several types of thin-film materials.

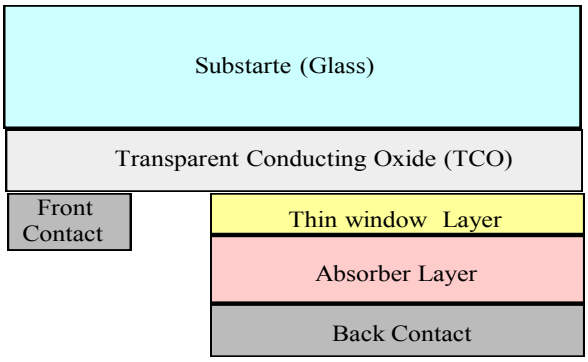

Figure 2-15: Schematic diagram of thin film solar cell

Amorphous silicon: This material has a significant advantage of higher absorption coefficient, about 40 times than that of crystalline silicon. It can be deposited on a low cost substrate and the manufacturing process requires low temperature and therefore less energy. It has lower material and manufacturing costs. Amorphous hydrogenated silicon (a-Si:H) has been widely used by the Japanese to power small consumer goods such as watches and calculators [22]. This material is a non-crystalline for silicon and does not form a regular crystal structure, but an irregular network. The material is highly defective even with hydrogenation, so the minority carrier lifetimes are very low resulting in low charge collection efficiency. A major drawback of this material is that it degrades under sun exposure, a mechanism called the Staebler-Wroski effect.

Cadmium Telluride (CdTe) : This is one of the most promising thin film solar cells. The material is a poly-crystalline semiconductor compound made of cadmium and tellurium. CdTe has the lowest production cost among the current thin-film technologies. Low-cost soda-lime glass is used as the substrate. The manufacturing processes have greatly

improved over the past few years. Though in 2003 CdTe thin film was a negligible contributor to total market of PV, it emerged rapidly in past decade [5]. From Figure 2-16 of comparative market scenario of various PV technology in 2008 and 2009 , it is clear that CdTe thin film technology will soon take a dominant position in PV market[25]. The CdS film is grown either by chemical bath deposition (CBD), close space sublimation (CSS), chemical vapor deposition (CVD), sputtering, or vapor transport deposition (VTD). This material has a very high absorption coefficient.

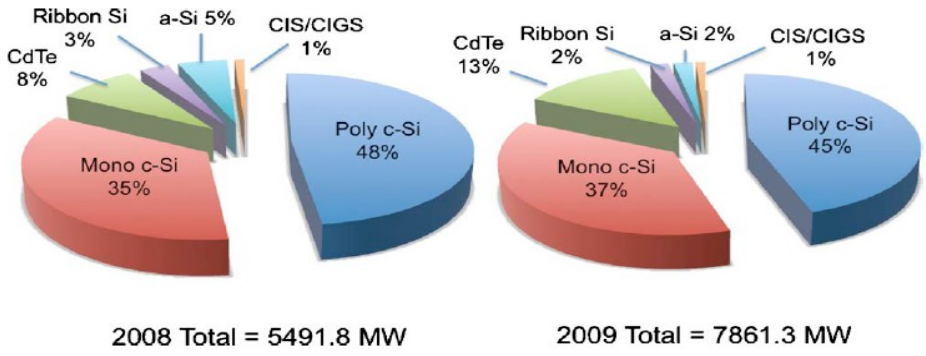

Figure 2-16: Market size and the share held by various PV technologies in 2008 and 2009[25].

Copper Indium Gallium Selenide (CIGS): CIGS is a polycrystalline semiconductor compound of Copper, Indium, Gallium and Selenium, and has been a major research area in the thin film industry. It is another promising material for thin-film solar cells. It can achieve high energy conversion efficiency and does not suffer from outdoor degradation problem and has demonstrated that thin film PV cells are a viable and competitive choice for the solar industry in the future. This material also has a high absorption coefficient

and only 0.5 micrometers needed to absorb 90% of the solar spectrum. However CIGS production involve with very complex material making process and difficult to manufacture. Moreover its manufacturing process involves hydrogen selenide, an extremely toxic gas raising safety concerns.

2.7 Performance Comparison of Different PV Materials

The future of the Photovoltaic industry is promising as the efficiency of the cell and sub modules continues to increase. The table 2-1 shows the most recent confirmed efficiency of cells measured under the global AM 1.5 spectrum (1000 W/m^2) at 25^0 C for various photovoltaic materials [26]. As technology and manufacturing processes continue to improve higher efficiencies are expected in the near future.

Table 2-1 : Confirmed terrestrial module efficiencies measured under global AM 1.5 spectrum

Material	**Efficiency**	**V_{OC}** (V)	**J_{SC}** (mA/cm^2)	**Fill Factor (%)**
Si (crystalline)	25.0 ± 0.5	0.706	42.7	82.8
Si (Multi crystalline)	20.4 ± 0.5	0.664	38	80.9
Si (Thin film polycrystalline)	16.7 ± 0.4	0.645	33	78.2
GaAs(thin film)	26.1 ± 0.8	1.045	29.6	84.6
GaAs(multicrystalline)	18.4 ± 0.5	0.994	23.2	79.7
CIGSS	19.4 ± 0.6	0.716	33.7	80.3
CdTe	16.7 ± 0.5	0.845	26.1	75.5
Si(amorphous)	9.5 ± 0.3	0.859	17.5	63.0
Si (nano crystalline)	10.1 ± 0.2	0.539	24.4	76.6

Solar cells based on bulk polycrystalline Si are likely going to remain dominant for the next decade. Thin-film technologies are maturing fast and may soon challenge the market share of crystalline Silicon devices. The dominant future technology will be determined largely by material availability and costs.

2.8 Charge Trapping in poly Crystalline Materials

A polycrystalline material is composed of many micro crystallites randomly oriented in different directions and joined together by grain boundaries as shown in Figure 2-17. Grain boundary which is the meeting place of differently oriented crystals is a complex structure, consisting of a few atomic layers of disordered atoms. Atoms in the grain boundary represent a transitional region and cannot follow their normal bonding tendency due to sudden changes of the crystal orientation across the boundary. As atoms cannot follow the crystalline pattern on either side of the boundary several crystallographic defects such as dislocations, vacancies, interstitials, dangling bonds, and distorted bond angles can be originated at the grain boundaries.

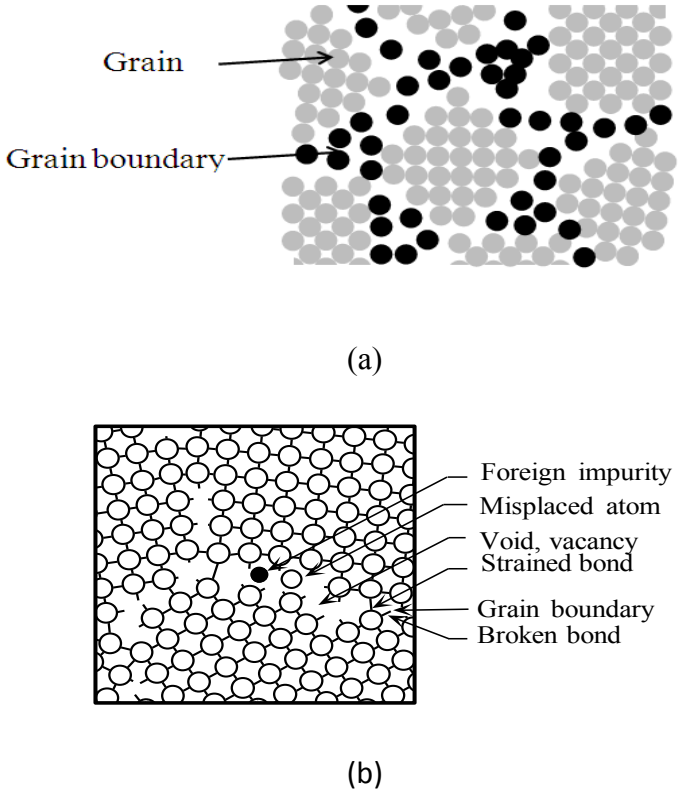

Figure 2-17: (a) The grain structure of polycrystalline solids. (b) The grain boundaries have impurity atoms, voids, misplaced atoms, and broken and strained bonds [27]

Electronic states formed at the grain boundaries due to inter-atomic bonding irregularities. These electronic states may have energies in the bandgap and these intra band gap states act as a trap centers for carriers. The trapping states of grain boundary traps carriers when attempting to move from one grain to other and create a space charge region (SCR) near the grain boundary. This space charge region altered electric field orientation.

2.9 Existing Models for *J/V* Characteristics of Thin film Solar Cells

Modern polycrystalline cells are complicated structures and the effects of some particular phenomenon, mechanism or material parameters are often not straight forward. Modeling can be used to provide insight, to interpret measurements and to assess the potential merits of a cell structure. For many years researchers are working to find a suitable model to explain the dependence of photocurrent on output voltage of a thin film solar cell. To get the resultant current for a particular voltage, dark current (forward bias current) need to sum up with calculated photocurrent. Several model developed to describe the J/V characteristics of thin film solar cell. Here we will discuss few models.

2.9.1 Misiakos's Model

K. Misiakos et al [13] describe two different models to calculate photocurrent in a amorphous silicon p-i-n solar cell. One model is for strongly absorbed light and another model is uniformly absorbed light.

For strongly absorbed light: In Misiakos's photo current for strongly absorbed light expressed as

$$J_{ph} = qP_F \frac{2\alpha\left(\frac{1}{L_E^2}+\frac{1}{L^2}\right)^{\frac{1}{2}}}{\alpha^2 + 2\frac{\alpha}{L_E} - \frac{1}{L^2}} \times \frac{\exp\left(\frac{W}{L_2}\right)}{1-\exp\left[W\left(\frac{1}{L_2}-\frac{1}{L_1}\right)\right]} \tag{2.11}$$

Where, $L_E = 2\left(\frac{kT}{q|F|}\right)$, $L = (D\tau)^{\frac{1}{2}}$ is diffusion length, P_F is the photon flux density, L_1 and L_2 is define as

$$L_1 = \left[\frac{1}{L_E} + \left(\frac{1}{L_E^2}+\frac{1}{L^2}\right)^{\frac{1}{2}}\right]^{-1}, \quad L_1 = \left[\frac{1}{L_E} - \left(\frac{1}{L_E^2}+\frac{1}{L^2}\right)^{\frac{1}{2}}\right]^{-1} \tag{2.12}$$

For uniformly absorbed light: Photo current for uniformly absorbed light expressed as

$$J_{ph} = qG\left\{l_{cu}\left[1-\exp\left(-\frac{W}{l_{cu}}\right)\right] - \left(\frac{kT}{q}|F|\right) \times \left[-2 + 2\exp\left(-\frac{W}{l_{cu}}\right) + 2\exp\left(-\frac{W}{l_{cu}}\right)\right]\right\} \tag{2.13}$$

Where, $l_{cu} = |F|\mu_p\tau_p$, is limiting carrier collection length , G is generation rate ,

W is the width of the devices, $|F| = \frac{(V_{bi} - V)}{W}$ is the electric field.

Limiting carrier is define as carrier with the least photo collected current .In this model it is needed to choose hole or electron as limiting carrier .

Assumptions and limitation: The assumptions and limitation of Misiakos's model are as follows:

a) Two separate model for strongly absorbed light and uniformly absorbed light.

b) In each model, it is needed to define a limiting carrier. Limiting carrier varies with device structure[13]

c) The electric field is uniform

2.9.2 Taretto's Model

K. Taretto [15] developed a closed form expression for the current-voltage characteristics of p-i-n solar cells. In this model the current density J in A/cm^2 is given by

$$J = \frac{qn_{po}D}{W} J_S \tag{2.14}$$

Where

$$J_S = 2S_S(C_1 + C_2 + G_S + n_S - 1) + \frac{1}{L_S^2}\left[\frac{C_1(\exp(\lambda_2/2) - 1)}{\lambda_2/2} - \frac{C_2(1 - \exp(\lambda_1/2))}{\lambda_1/2} - \frac{(n_s - 1)(1 - \exp(-V_{SO}/2))}{-V_{SO}/2}\right]$$

$$C_1 = -\frac{\exp(-\lambda_2/2)}{A_3} \times [A_1(\lambda_2 + S_s) + A_2 \exp(\lambda_1/2)]$$

$$C_2 = -\frac{\exp(-\lambda_2/2)}{A_3} \times [A_1(\lambda_1 + S_s) + A_2 \exp(\lambda_2/2)]$$

the quantities A_1, A_2 and A_3 are defined by

$$A_1 = n_s(1/2) - G_S - n_s \exp(-V_{s0}/2) \ ,$$

$$A_2 = n_s(S_s - V_S - n_s + V_{s0}) - S_s + G_s(S_s - V_{s0}) \ , \text{ and}$$

$$A_3 = -\lambda_2 + S_s + (\lambda_1 + S_s) \times \exp(\frac{\lambda_1 - \lambda_2}{2}) .$$

The dimensionless λ_1 and λ_2 are given by

$$\lambda_{1,2} = -\frac{V - V_{bi}}{2V_t} \pm \sqrt{\left(\frac{W}{L}\right)^2 + \left(\frac{V - V_{bi}}{2V_t}\right)^2}$$

Here, $V_{s0} = -V_{bi}/V_t$, distance x_s, electron concentration n_s, diffusion length L_s, surface recombination velocity S_s, potential drop V_s, and generation rate G_s are scaled.

Assumptions and limitation: The following assumptions and limitations are belongs to this model

a) This model has lot of parameters and complex for calculating photocurrent.

b) The electric field in the intrinsic layers is uniform

c) The current density $J < J_{CR}$ is satisfied, where J_{CR} is a critical current density and defined as

$$J_{CR} = \frac{kT\mu_n N_C}{\int_{x=0}^{x=W/2} \exp\left(\frac{E_C(x)}{kT}\right) dx},$$

which contain the electron mobility μ_n, the electron density of state N_C, and the energy $E_C(x)$ at the conduction band edge.

d) The photo generation rate is homogeneous within the i-layer

e) The carrier mobilities μ and lifetimes τ have the same values for electrons and holes.

2.9.3 Model Based on Voltage Dependent Collection Efficiency

Hegedus et al. [16] reviewed three models to describe the current-voltage (J-V) characteristics in a thin film solar cell. In this three models it is assumed that photo generated current $J_L(V)$ is equal to the product of a constant current density J_{LO} and a voltage dependent charge collection efficiency $\eta_c(V)$ [28] [29] [30]. That is,

$$J_L(V) = J_{LO} \times \eta_C(V) \tag{2.15}$$

where J_{LO} is the maximum photocurrent with complete collection. It is assumed that J_{LO} is the photo current obtained at sufficiently large reverse bias and linearly dependent on light intensity but not on the voltage. $\eta_c(V)$ is the voltage dependent collection efficiency and varies from 1 at reverse bias to 0 at some forward bias V_O.

The net current density from a solar cell is

$$J(V) = J_d(V) - J_L(V) \tag{2.16}$$

Where $J_d(V)$ is the forward diode current.

When $\eta_c(V)$ =1 at all voltages resultant photocurrent can be calculated by the principle of superposition where the light current equal to downward shifted dark current by a constant photocurrent , J_{SC}.

Three different models based on voltage dependent photocurrent collection efficiency $\eta_c(V)$ are given below.

Model-1: In the first model both interface recombination and drift collection losses are considered with the interface collection factor (ICF). The voltage dependent charge collection efficiency expressed as [31][32][29]

$$\eta_C(V) = \frac{\mu F_0(V)}{S + \mu F_0(V)} \tag{2.17}$$

Here μ is the minority carrier mobility, $F_0(V)$ is the field at the interface, and S is the surface recombination velocity. For CdTe solar cell $F_0(V)$ is not well established however for a *p-n* heterojunction it can be written as

$$F_0(V) = \left[\frac{2qN_A}{\varepsilon}(V_{bi} - V) \right]^{1/2} \tag{2.18}$$

Here N_A is the doping concentration of the absorber layer. It has four fitting parameter namely μ, S, N_A and V_{bi},

Model-2: In the second model voltage dependent charge collection efficiency dependent on depletion width $W(V)$ and a diffusion length L [33].

$$\eta_C(V) = 1 - \frac{\exp\{-\alpha(\lambda)W(V)\}}{1+\alpha(\lambda)L} \tag{2.19}$$

Where, α (λ) is the wavelength-dependent absorption coefficient. Voltage dependent depletion width $W(V)$ determines the voltage dependence of the photocurrent collection and expressed as

$$W(V) = \left[\frac{2\varepsilon}{qN_A}(V_{bi} - V)\right]^{1/2} \tag{2.20}$$

This model also has four fitting parameter namely $\alpha(\lambda)$, L, acceptor carrier density N_A and built in potential V_{bi}.

Model-3: In this model it is assumed that depletion region recombination is the dominant collection loss mechanism, means diffusion from a neutral region is negligible due to too small diffusion length and all light is absorbed within the high field region [16]. Voltage dependent collection efficiency in a-Si *p-i-n* solar cells expressed as [34][13],

$$\eta_C(V) = X(V)\left[1 - \exp\left(-X(V)^{-1}\right)\right] \tag{2.21}$$

Where

$$X(V) = \frac{\mu\tau V_{bi}}{d^2}\left(1 - V/V_{bi}\right) \tag{2.22}$$

$\mu\tau$ is the minority carrier mobility lifetime product , d is the i-layer thickness. In this model $\mu\tau$, d, V_{bi} , V_{bi} are the fitting parameters.

2.10 Limitation of Existing Models

As described earlier K. Misiakos's and K. Taretto models based on some impractical assumptions and are not suitable to use commonly to determine the J-V characteristics curve of thin film solar cell. Hegedus et al. had shown that the most successful model calculates the photocurrent by considering carrier drift and utilizing Hecht collection efficiency formula (model 3 above) in the nearly intrinsic absorber layer [16]. The model has made an impractical assumption that all the carriers are generated at the top interface of the absorber layer for all incident photons and used a number of fitting parameters such as maximum photocurrent with complete charge collection, reverse saturation current, effective attenuation coefficient, series resistance and carrier ranges.

All the models discussed above considered uniform electric field distribution in the intrinsic or depleted region of the absorber layer. Electric field can be assumed uniform only for low doped absorber layer. However, electric field distribution is non uniform in all practical devices due to presence of on space and trapping charge density. For non uniform electric field all the above mentioned models are not applicable. Therefore it is necessary to develop a suitable model to describe the J-V characteristics of thin film solar cell which can addressed both uniform and non uniform electric field.

2.11 Summary

Solar cell physics and necessary theoretical background regarding the modeling of thin film solar cell have been briefly discussed in this chapter. These concepts will be very helpful to understand our model. We also discuss some existing models and their limitations in this chapter. In next chapter, we are going to discuss our proposed model for the current-voltage characteristics of thin film solar cells.

CHAPTER 3 : NUMERICAL MODELING CONSIDERING SPACE CHARGE EFFECT

3.1 Introduction

There has been an active theoretical and experimental research to improve the performance of thin film solar cells and modeling the current-voltage (J-V) characteristics curve under illuminated condition. All existing models assumed uniform electric field and photo generated carriers flow due to drift throughout the absorber layer which is reasonably valid for low doped absorber layer. For high level of space or trapped charge density electric field is non uniform and the profile of electric field depends on the charge density in the absorber layer. The voltage dependent electric field near the top interface of the absorber layer is higher than that of near the bottom interface; the photo generated carriers will drift with higher velocity near the top interface compared to that near the bottom interface. Even, Electric field collapse somewhere in the absorber layer when space or trapped charge density exceeds a certain limit. In that case, photo generated carriers in the depleted region of absorber layer are driven by drift and photo generated carriers in the outside of depleted region are driven by diffusion.

3.2 Thin film Solar Cell Considering Space Charge Effect

In a thin film CdTe or CIGS p-n junction solar cells, the width of n side is very thin and doping concentration is very high, on the other hand the width of p side is much greater than n side and doping concentration in the p side is much lower compare to the n side.

So electric field in p side can be assumed uniform as long as space or trapped charge density is low. However practically the electric field in p-side is not fully uniform, it varies due to the presence of space or trapped charge. The deviation from uniformity is no more negligible if space charge or trapped charge density is high. Non uniform electric field exist in the depleted region of the absorber layer and even electric field may collapse somewhere in the absorber layer if space or trapped charge density exceed a limit. Photo generated carrier in the absorber layer are collected by drift in the depleted region and by diffusion in zero electric field region as shown in Figure 3-1. The point where electric field collapses depends upon magnitude of space or trapped charge density. With the increase of space or trapped charge density electric field profile become steeper and collapse in shorter distance of absorber layer.

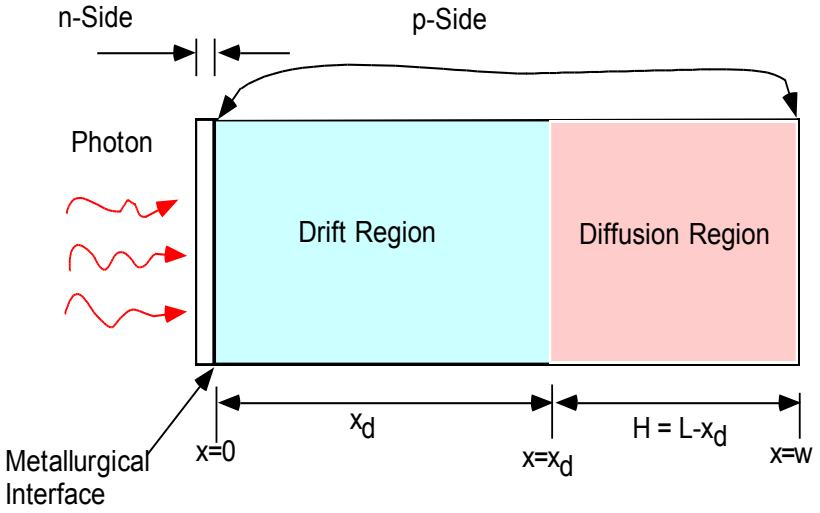

Figure 3-1: Schematic diagram of thin film solar cell in non uniform electric field

In this model, we consider the upward electrode is on top of a very thin n region, the bottom electrode at the end of P region and sunlight passes through the top electrode. Due

to the very thin n layer light mostly absorbed in p-side. In the drift region of p-side photo generated electrons drift towards upward electrode and hole drift towards bottom electrod due to electric field. Photo generated excess carrier in bulk region of p side will flow due to diffusion. Total photo generated current will be the summation of drift current and diffusion current.

3.3 Uniform Electric Field

Electric field is defined as the electric force per unit charge. The direction of the field is taken to be the direction of the force it would exert on a positive test charge. The electric field is outward from a positive charge and in toward a negative point charge. In a semiconductor junction the electric field can be deduced from the potential barrier. Electric field distribution within the transition region can be calculated with the absorber layer width. Poisson's equation which relates the gradient of the electric field to the local space charge at any point x

$$\frac{\partial F(x)}{\partial x} = -\frac{\rho(x)}{\varepsilon} \tag{3.1}$$

Where, $\rho(x)$ is charge density and ε is permittivity of the semiconductor. For low doped case the gradient of electric field can be assumed zero and electric field is practically uniform in the transition region as shown in Figure 3-2. In this case average electric field can calculate simply dividing the terminal voltage with the device length. The magnitude of uniform electric filed in a depletion region is as follows:

$$F = \frac{V_{bi}}{W} \tag{3.2}$$

Where W is width of depleted region and V_{bi} is the built-in potential.

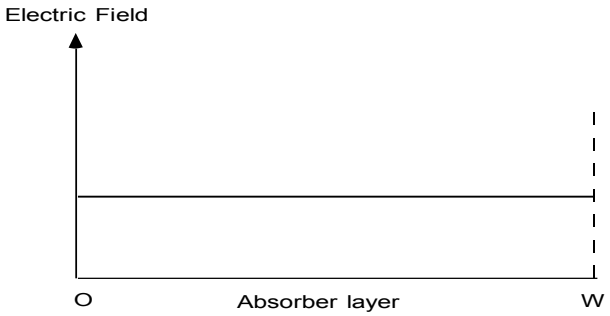

Figure 3-2: Uniform distribution of electric field in the absorber layer

For a case of thin film solar cell with output voltage V, electric field will be

$$F = \frac{V_{bi} - V}{W} \tag{3.3}$$

If thin film solar cell has a series resistance R_S and current J_s the uniform electric field distribution can be modified as

$$F = \frac{V_{bi} - (V + J_S R_S)}{W} \tag{3.4}$$

3.4 Non Uniform Electric Field

For high level of doping the gradient of electric field is not negligible that means electric field is not uniform in the absorber layer. In this case the electric field varies with the

distance in the absorber layer. Electric field variation depends upon the distribution of space or trapped charge density and three different profile of electric field profile are possible.

Case 1: For uniform distribution of space charge density electric field vary linearly with distance in the absorber layer and profiles is triangular as shown in Figure 3-3 [35]. Slope of electric field depends upon space charge density.

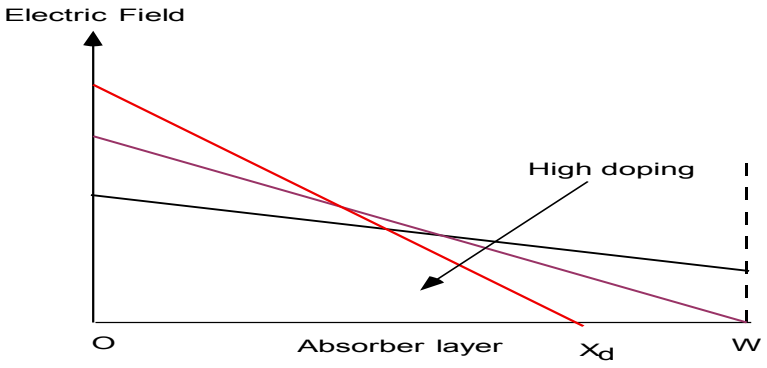

Figure 3-3: Linear variation of electric field in absorber layer

Case 2: For linear distribution of space or trapped charge density electric field vary exponentially in the absorber layer as shown in Figure 3-4. Here we considered maximum electric field exist at the interface x=0; and due to presence of negative space or trapped charge electric field decrease exponentially and collapse at some point x_d of the absorber layer.

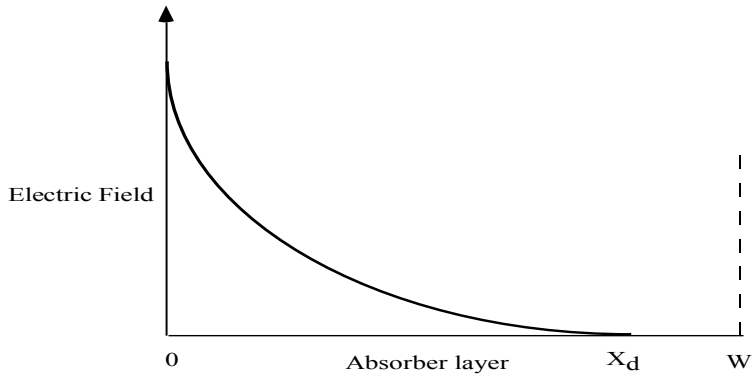

Figure 3-4: Exponential variation of electric field in absorber layer

Case 3: Trapped charged in the absorber layer may be positive or negative. Due to different type of trapped charge the electric field in the absorber layer may vary as like as shown in Figure 3-5. In this case separate mathematical expressions are required to define electric field in every part of the absorber layer.

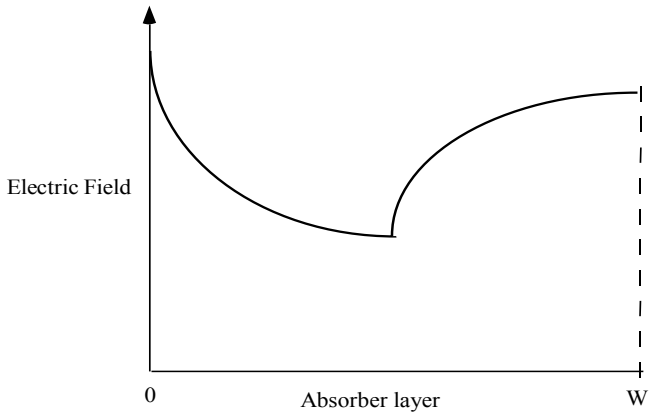

Figure 3-5: Random variation of electric field in the absorber layer

3.5 Modeling of J/V Characteristics

Due to very short diffusion length and very thin width current contribution by the photon absorption in the highly doped top *n* layers is negligible. The photo generated electrons and holes are drifted in opposite directions by the built-in electric field in the depleted region of absorber layer. Electrons drift towards the radiation-receiving contact (top contact) and holes drift towards the bottom contact of the solar cells. The photo generated electrons in outside of depleted region driven by diffusion. Here we proposed a model which address both drift and diffusion current of thin film solar cell considering effects of space or trapped charge density in the absorber layer.

The following assumptions are made in the present model:

(i) The thermal generation of charge carriers is negligibly small because of high bandgap materials.

(ii) The diffusion of carriers is negligible compared with their drift in the depleted region of absorber layer.

(iii) Mobility μ and lifetime τ are assumed to be constant to each type of carriers (holes and electrons) during movement in the absorber layer.

(iv) In the model the effect of shunt resistance on current voltage characteristics is neglected.

(v) In the model the thin film solar cell structural sequence assumed as of top contact, very thin n^+ layer, absorber p layer and bottom contact.

3.5.1 Continuity Equation of the System

The steady-state continuity equation for the electrons that drift towards the top electrode is,

$$\frac{\partial n}{\partial t} = \mu_n \left(F \frac{\partial n}{\partial x} + n \frac{\partial F}{\partial x} \right) - \frac{n}{\tau_n} + G e^{-\alpha x} = 0 \qquad (3.5)$$

the steady-state continuity equation for the hole that drift towards the bottom electrode is,

$$\frac{\partial p}{\partial t} = -\mu_p \left(F \frac{\partial p}{\partial x} + p \frac{\partial F}{\partial x} \right) - \frac{p}{\tau_p} + G e^{-\alpha x} = 0 \qquad (3.6)$$

Where n is the photo generated electron concentration drifting towards the upper electrode, p is the photo generated hole concentration drifting towards the bottom electrode, μ_n and μ_p are the mobility of electron and hole respectively, τ_n and τ_p are the lifetime of electron and hole respectively, α (λ) is the absorption coefficient of the materials, λ is the photon wavelength, x is depth in the p side from the interface of p-n junction where $x = 0$, G is the carrier generation rate at the interface $x = 0$. F represents the electric field in the absorber-layer.

3.5.2 Steady-State Carrier Concentration

To find steady state carrier concentration electron-hole pair generation rate for thin film is calculated as

$$G(\lambda) = \alpha(\lambda) e^{-\alpha_1 d} \left[1 - R(\lambda)\right] \lambda I_0(\lambda) / hc \tag{3.7}$$

Where, c is the speed of light, h is the Plank constant, I_0 is the intensity of the solar spectra (W/cm^2-nm), R is the total reflection and scattering loss factor, α is the absorption co-efficient of main absorber layer, α_1 is the absorption coefficient and d is the thickness of the thin top semiconductor layer . The other losses include shading from the grid, absorption in the top SnO_2 layer, and incomplete electron-hole pair (EHP) generation in the absorber layer [10].

To determine the steady state carrier concentration under non uniform electric field, continuity equations have to be solved by putting electric field expression which value is changed with the distance along with the width of absorber layer. Continuity equations considering variable electric field have no close form solution and need to be solved numerically.

To find electric field expression we start with the Poisson's equation,

$$\frac{\partial F(x)}{\partial x} = -\frac{\rho(x)}{\varepsilon}$$

Here $\rho(x)$ is the steady state space charge density.

Uniform Distribution of Space Charge: For uniform distribution of Space charge density in a thin-film solar cell the Poisson's equation become

$$\frac{\partial F(x)}{\partial x} = -\frac{q}{\varepsilon} N_a \tag{3.8}$$

Where, Na is acceptor concentration in p side.

Applying boundary condition; potential at x = 0 is equal to built in potential V_{bi} , the electric field expression became

$$F(x) = -\frac{q}{\varepsilon} N_a x + \frac{qN_a}{2\varepsilon} x_d + \frac{V_{bi}}{x_d} \tag{3.9}$$

Here, x_d is the distance from n-p interface where electric field collapse. By applying triangular area formula the value of x_d found as, $x_d = \sqrt{\frac{2V_{bi}\varepsilon}{qN_a}}$

The above electric field equation can be written as

$$F(x) = mx + C$$

Where, $m = -\frac{q}{\varepsilon} N_a$ and $C = \frac{qN_a}{2\varepsilon} x_d + \frac{V_{bi}}{x_d}$

By putting $F(x) = mx + C$, the steady state continuity equation of electron became

$$\frac{\partial n}{\partial x} + \frac{Un}{mx + C} = \frac{Q \exp(-\alpha x)}{mx + C} \tag{3.10}$$

Where, $U = m - \frac{1}{\mu_n \tau_n}$, and $Q = -\frac{G}{\mu_n}$.

In the same way the steady state continuity equation for hole in drift region of p side is

$$\frac{\partial p}{\partial x} + \frac{Zn}{mx + C} = \frac{S \exp(-\alpha x)}{mx + C} \tag{3.11}$$

Where, $Z = m + \frac{1}{\mu_p \tau_p}$, and $S = \frac{G}{\mu_p}$

Equations 3-10 and 3-11 have to be solved to determine the carrier concentrations in the depleted region. There is no close form solution of these equations. Drifting electrons and holes concentration in the absorber layer are determined by solving the equations numerically. Boundary condition for drifting electrons concentration is *n=0* at the beginning of the depleted region (x =0) and boundary condition for drifting holes is *p=0* at the end edge of depleted region ($x = x_d$), where x_d is the width of the depleted region in light absorber layer.

Non uniform Distribution of Space Charge: For some materials electrons holes are trapped in the absorber layer and effectively altered the electric field distribution. If the spatial distribution of trapped charge density in absorber layer is known, the Poisson's equation can write as

$$\frac{\partial F(x)}{\partial x} = -\frac{q}{\varepsilon}(p_t - n_t) \tag{3.12}$$

Where p_t is trapped hole density and n_t is trapped electron density.

The trapped hole and electron charge density can be expressed as [36][37]

$$p_t = B \times \frac{\exp(-\alpha x) - \exp\left(-\frac{x}{\mu_p \tau_p F_0}\right)}{1 - \alpha \mu_p \tau_p F_0} \tag{3.13}$$

$$n_t = B \times \frac{\exp(-\alpha x) - \exp\left(-\frac{L-x}{\mu_n \tau_n F_0}\right) \times \exp(-\alpha L)}{1 + \alpha \mu_n \tau_n F_0} \tag{3.14}$$

Where, $B = \phi_0 \left(\frac{1 - \exp(-\alpha x_d)}{x_d} \right)$, $\phi_0 = e^{-\alpha_1 d} \left[1 - R(\lambda)\right] \lambda I_0(\lambda) / hc$ is photon flux density and x_d is the width of depleted region in the absorber layer.

If $\mu_p \tau_p F_0 \gg$ and $\alpha x < 1$ then spatial distribution of trapped charge density in the absorber become linear.

The Poisson's equation become

$$\frac{\partial F(x)}{\partial x} = \frac{qB}{\varepsilon} \left[\frac{\exp(-\alpha x) - \exp\left(-\frac{x}{\mu_p \tau_p F_0}\right)}{1 - \alpha \mu_p \tau_p F_0} - \frac{\exp(-\alpha x) - \exp\left(-\frac{L-x}{\mu_n \tau_n F_0}\right) \times \exp(-\alpha L)}{1 + \alpha \mu_n \tau_n F_0} \right] \tag{3.15}$$

Steady state distribution of carrier can be calculated by simultaneous solving continuity equation and Poisson's equation.

3.5.3 Drift Photo Current

Drift photocurrent density due to electron,

$$j_{nt}(\lambda, V) = \frac{q \mu_n}{x_d} \int_0^{x_d} n.F dx \tag{3.16}$$

Where , q is charge of an electron, μ_n is the mobility of electron, x_d is the width of depleted region , n is steady state electron concentration, F is electric field.

Similarly drift photocurrent density due to hole

$$j_{pt}(\lambda,V)=\frac{q\mu_p}{x_d}\int_0^{x_d} p.Fdx \qquad (3.17)$$

Where , μ_p is the mobility of hole, x_d is the width of depleted region , p is steady state hole concentration, F is electric field.

From the above equation j_{nt} (λ, V) and $j_{pt}(\lambda, V)$ can be calculated by numerical integration.

Total drift photocurrent density,

$$j_t(\lambda,V)=j_{nt}(\lambda,V)+j_{pt}(\lambda,V) \qquad (3.18)$$

3.5.4 Diffusion Photo Current in Zero Electric Field Region of the Absorber Layer

If uniform electric field is consider throughout the absorber layer width, current flow mainly due to drift. If space or trapped charge density is high enough then the electric field become zero somewhere in the absorber layer. In the region of zero electric field current will flow due to diffusion only.

In our model n side is highly doped and very thin so there is no bulk region in n side. In the bulk region of p side where no electric field exists, excess photo generated electron will follow due to diffusion.

Steady state continuity equation for excess minority electron in the bulk p region;

$$\frac{\partial n}{\partial t} = D_n \frac{\partial^2 n}{\partial x} - \frac{n}{\tau_n} + G\exp(-\alpha x) = 0 \tag{3.19}$$

The equation can be write as

$$\frac{\partial^2 n}{\partial x^2} - \frac{n}{L_n^2} = -\frac{G}{D_n}\exp(-\alpha x) \tag{3.20}$$

Where, D_n is diffusion co-efficient and $L_n = \sqrt{D_n \tau_n}$, diffusion length of electron.

Necessary boundary conditions to solve the equation are [38];

At the end of depletion region or beginning of diffusion region, the excess carrier density is zero due to the electric field in the depletion region, that means

$n=0$, at $x = x_d$, and

$$S_n n = -D_n \left.\frac{\partial n}{\partial x}\right|_{x=L} \tag{3.21}$$

Where, S_n is surface recombination velocity and L is the length of the absorber layer.

Using these boundary conditions the electron distribution in a p side bulk region is

$$n(x,\lambda) = \frac{G\tau_n \exp(-\alpha x_d)}{\alpha^2 L_n^2 - 1}\left[Cosh\frac{x - x_d}{L_n} - \exp\left(-\alpha\left(x - x_d\right)\right) - \frac{\frac{S_n L_n}{D_n}\left(Cosh\frac{H}{L_n} - \exp(-\alpha H)\right) + Sinh\frac{H}{L_n} + \alpha L_n \exp(-\alpha H)}{\frac{S_n L_n}{D_n} Sinh\frac{H}{L_n} + Cosh\frac{H}{L_n}} \times Sinh\frac{x - x_d}{L_n}\right] \tag{3.22}$$

Where $H=L- x_d$, the length of zero electric field region in P side.

The diffusion photocurrent due to electrons collected at the end of depletion region at $x=x_d$ is

$$j_{dn} = qD_n \left.\frac{dn}{dx}\right|_{x=x_d} \tag{3.23}$$

From the above equation the diffusion current due to photo generated carriers in the zero electric field region of the absorber layer can be expressed as

$$j_d(x,\lambda) = \frac{qGL_n \exp(-\alpha x_d)}{\alpha^2 L_n^2 - 1}\left[\alpha L_n - \frac{\frac{S_n L_n}{D_n}\left(Cosh\frac{H}{L_n} - \exp(-\alpha H)\right) + Sinh\frac{H}{L_n} + \alpha L_n \exp(-\alpha H)}{\frac{S_n L_n}{D_n} Sinh\frac{H}{L_n} + Cosh\frac{H}{L_n}}\right] \tag{3.24}$$

3.5.5 Net Current in Solar Cell

Photo generated current density at any incident photon wavelength will be summation of drift and diffusion current density

$$j_L(\lambda, V) = j_t(\lambda, V) + j_d(\lambda, V) \tag{3.25}$$

The total photo generated current density is obtained by integrating over all incident photon wavelengths of the solar spectrum

$$J_L(V) = \int_0^\infty j_L(\lambda, V)\, d\lambda \tag{3.26}$$

The net current density from a solar cell is

$$J(V) = J_d(V) - J_L(V) \tag{3.27}$$

Where, $J_d(V)$ is the forward diode current.

3.5.6 Forward Diode Current

The forward diode current can be written as,

$$J_d(V) = J_0 \exp\left[\frac{q(V - JR_s)}{AkT}\right] \tag{3.28}$$

Where J_0 is the reverse saturation current density, A is the diode ideality factor, k is the Boltzmann constant, and T is the absolute temperature. For *p/n* junction with thin depletion region width minority carrier diffusion current will be dominant one and J_0 can be expressed as [39]

$$J_0 = \frac{qD_p p_{no}}{L_p} + \frac{qD_n n_{po}}{L_n} \tag{3.29}$$

However if the depletion region is thick, recombination current should be dominant over ideal diffusion current [40]. Therefore, the reverse saturation current density can be written as [41],

$$J_0 = \frac{qn_i W}{\sqrt{\tau_n \tau_h}} \tag{3.30}$$

Where, n_i is the intrinsic carrier concentration of the absorber layer.

3.6 Summary

In this chapter, we have discussed the proposed model for *J-V* characteristics simulation of thin film solar cells considering space charge effects. Total photo current is calculated considering drift current in the depleted region and diffusion current in the zero field region of the absorber layer. The present model only uses series resistance as fitting parameters and thus eliminates other fitting parameters such as carrier transport properties, reverse saturation current and effective attenuation coefficient. The actual solar spectrum is considered in our model. Moreover how the various parameters such as carrier transport properties, surface recombination velocity, temperature, absorber layer width, thickness of windows layer affect the J-V characteristics are also considered in the proposed model. In the next chapter, we will make theoretical analysis based on our proposed model and apply the model to various thin film solar cells. We will compare our results with the published experimental data.

CHAPTER 4 : RESULTS AND DISCUSSION

4.1 Introduction

The simulation result of our proposed model for thin film solar cell under non uniform electric model is presented in this chapter. Electric field profile in the absorber layer is analyzed with the variation of space charge density. Drift current due to photo generated carriers in the depleted region is calculated by solving continuity equation numerically. Diffusion current in the zero electric field region can be calculated from analytical expression. Net photo current at a particular voltage is calculated taking the effects of dark current. We analyzed the *J-V* characteristics of of thin film solar cells by varying space charge density, surface recombination velocity, temperature, carrier transport properties, absorber layer width and window layer thickness. The *J-V* characteristics of CdTe and CIGS based thin film are determined by applying our model and the model is verified by comparing with experimental data. The effect of series resistance on *J-V* characteristics are also evaluated in our model.The incident photon flux $I_0(\lambda)$ is taken as the air mass (AM) 1.5 global spectrum from the ASTM G-173-03 standard [42]. All analysis are done for uniform distribution of space charge density.

4.2 Electric Field Distribution in the Absorber Layer

The electric field throughout the absorber layer can be considered as constant for low space charge density $\left(N \le 10^{12}/cm^3\right)$. For small increase of space charge density $\left(N \approx 10^{13}/cm^3\right)$ the electric field decreases slightly along the distance of absorber

layer. Neglecting the small variation, the electric field profile can be assumed uniform throughout the absorber layer. In this case, the full absorber layer is depleted and all photo generated carriers in the absorber layer will be driven by the electric field and total photocurrent will be due to the drift mechanism.

For high space charge density $\left(N \geq 10^{14} / cm^3\right)$ the electric field varies significantly throughout the absorber layer and the variation become more dominant with the increase of space charge density. The magnitude of electric field is very high at the top edge of the absorber layer and gradually decreases along the absorber layer. The electric field collapses somewhere in the absorber layer. In this case, the electric field cannot be considered uniform in the depleted region of the absorber layer. The voltage dependent electric field near the top of the drift region is much higher than that near the bottom edge. The photo generated carriers will drift with a much higher velocity near the top edge compared to that near the bottom edge of drift region. To calculate actual drift current it is needed to be considered photo generated carriers in every point of drift region that are driven by the corresponding electric field. This can only be done by numerical method.

For some high space charge density electric field collapse somewhere in the absorber layer and no more exist throughout the absorber layer. Space charge density determines the point in the absorber layer, where electric field collapses. If space charge density increases electric field collapse in shorter distance, that means drift region width in the absorber layer shrinks with increase of space charge density. In the remaining part of the

absorber layer electric field is zero. So photo generated carriers in the zero electric field regions will flow only by diffusion.

Figure 4-1 shows the variation of electric field profile for various space charge density at an output voltage of 0.6 V. Here the absorber layer width $L = 3.5 \times 10^{-4}$ cm is considered. The electric field becomes steeper with the increase of space charge density. Electric field collapsed in a point of the absorber layer when space charge density crosses a limit. So photo generated carriers in the depleted region will flow due to drift and photo generated carriers in the zero electric field region will flow due to diffusion only. Total photocurrent will be summation of drift and diffusion current.

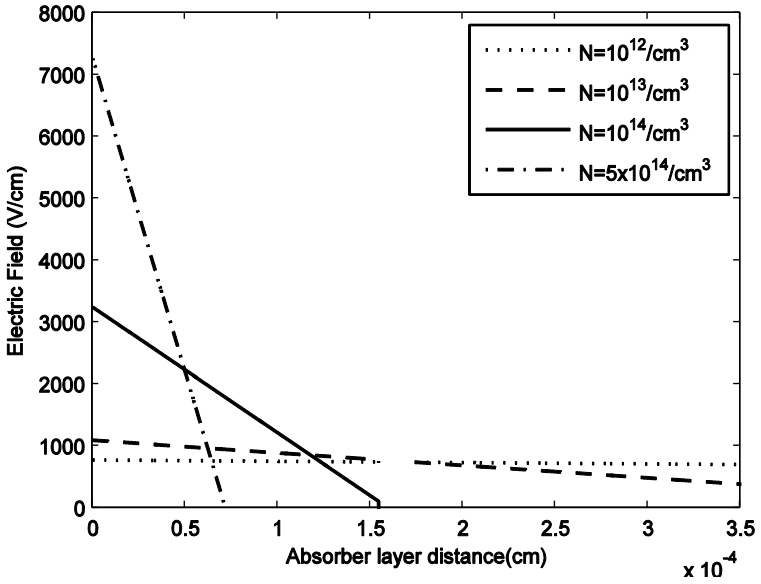

Figure 4-1: Electric field variation in the absorber layer for various space charge density (N) ,at output voltage V_{output} =0.6 V.

4.3 Carrier Concentration Profile in the Absorber Layer

Here the carrier concentrations profiles in the depleted region and in the zero electric field region of the absorber layer are analyzed. Width of the depleted region and zero electric field regions vary with space charge density and hence the carrier concentration profile also varies accordingly.

Figure 4-2 shows the electron concentration in the depleted region of the absorber layer for different space charge density. At low space charge density $\left(N \approx 10^{13} / cm^3\right)$ the whole absorber layer is depleted and electrons concentration exists everywhere in the absorber layer. In this case, the electron concentration at the top edge is very high due to uniform electric field distribution and exponential carrier generation by photon absorption. With the increase of space charge density the electric field become steeper and it is very high at the top of the absorber layer. Due to this high electric field, photo generated electrons at the top edge of the absorber layer drift swiftly towards top layer compared to the low electric field part of the depleted region. As a result electrons concentration at the top edge decreases sharply with the increase of space charge density.

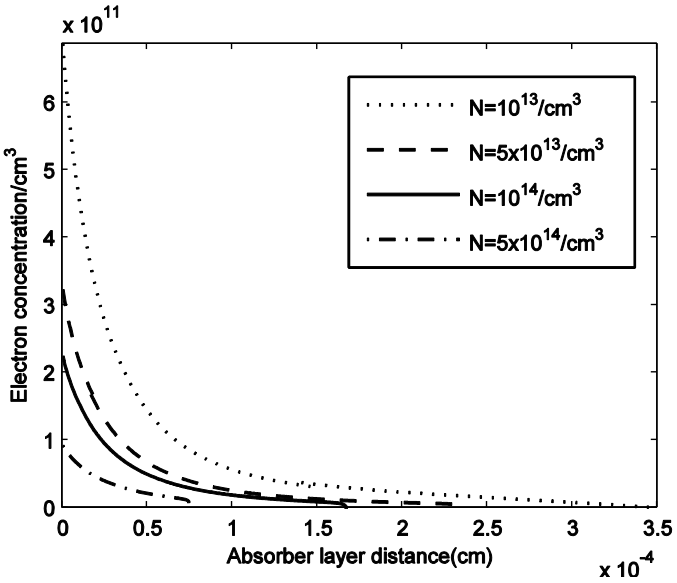

Figure 4-2: Electron concentration profile in the depleted region for different space charge density (N) at output voltage V_{output} =0.6 V

Figure 4-3 shows the hole concentration in the depleted region of the absorber layer for different space charge density. At low space charge density as electric field is uniform; uniform hole concentration exists everywhere in the absorber layer. At high space charge density, depleted region shrink and magnitude of electric field is very high at the top edge of the absorber layer. So hole drift swiftly towards bottom side. Therefore hole concentration at the bottom edge of depleted region decrease with the increase of space charge density.

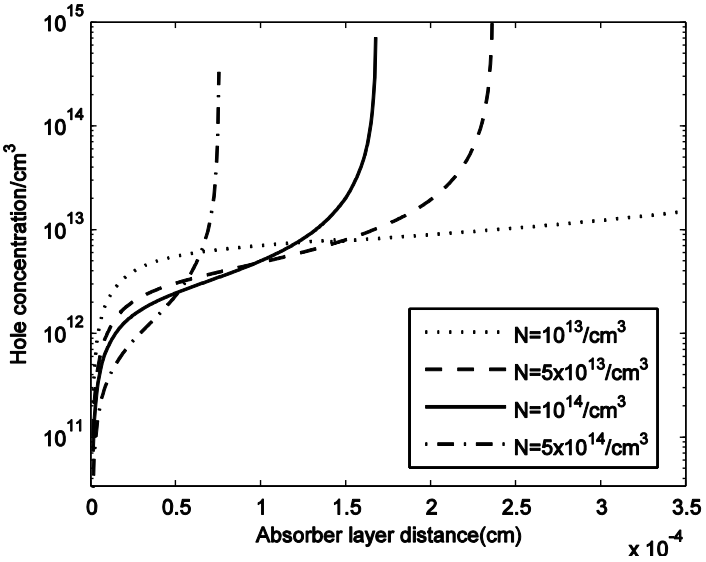

Figure 4-3: Hole concentration profile in the depleted region for different space charge density (N) at output voltage V_{output} =0.6 V

In the neutral p side the electric field is zero. The photo generated electrons in zero electric field flow due to diffusion and contribute to the photo current. Figure 4-4 shows the photo generated electron concentration in the zero electric field region of the absorber layer for different space charge density at a constant surface recombination velocity $S_n=10^7$ cm/s. With the increase of space charge density the width of zero electric field region increases and the diffused electron concentration also increases.

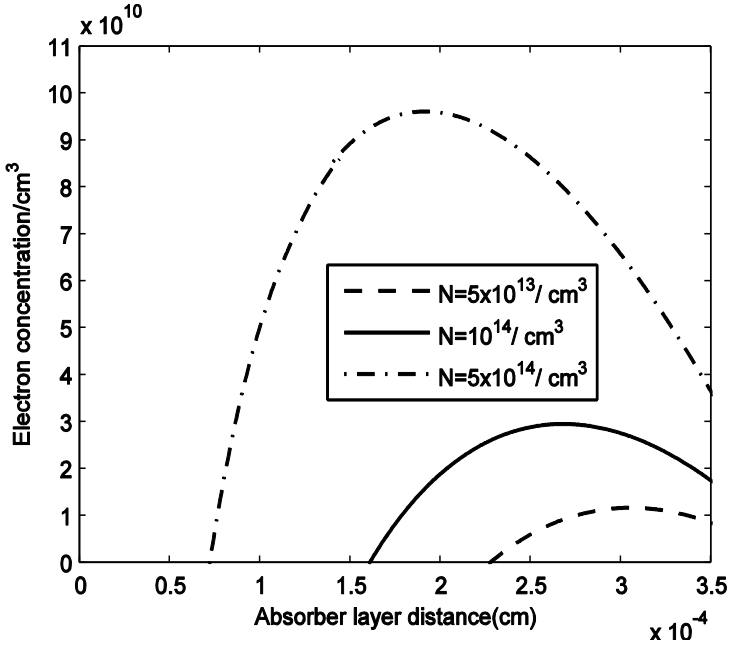

Figure 4-4: Electron concentration profile in neutral (zero electric field) p region for different space charge density (N) at output voltage V_{output} =0.6 V

Diffused electrons concentration profile changes with surface recombination velocity. Concentration of diffused electron in the bottom edge of the absorber layer highly depends upon surface recombination velocity. Figure 4-5 shows the diffused electron concentration for different surface recombination velocities at a constant space charge density of $N = 10^{14} / cm^3$. The diffused electron concentration at the bottom edge is decreases with increasing of surface recombination velocity due to more electrons recombination at the surface. So, low surface recombination velocity is desirable for better performance of solar cell.

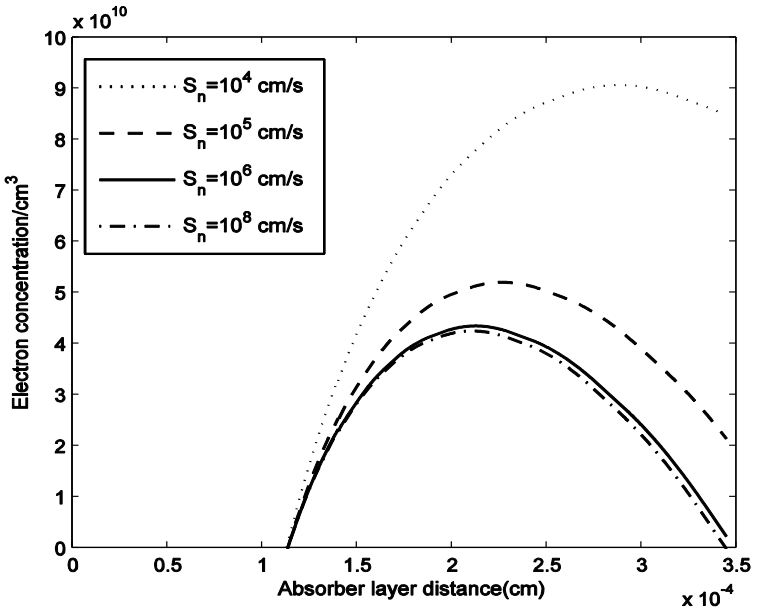

Figure 4-5: Electron concentration profile in neutral (zero electric field) p region for different surface recombination velocity (S_n) at output voltage V_{output} =0.6 V

4.4 Space Charge Effects on Drift and Diffusion Current

All existing models assumed uniform electric field throughout the absorber layer and considered the photocurrent is only due to drift of photo generated carriers and drift current does not change with space charge density. In fact the drift current itself changes significantly with space or trapped charge density in the absorber layer. The reason behind changing drift current with space charge density is due to the change of depleted region width and electric field profile.

Figure 4-6 shows the variation of drift current with voltage at different space charge densities. It is evident from the figure that in the low doped range ($N < 10^{14}$ / cm^3) the drift current does not change significantly with the change of space charge density. In the

case of low doping, the electric field variation is negligible and can be considered as uniform throughout the absorber layer. However for high doped case, the drift current decreases significantly with the increase of space charge density. These variations of drift current do not reflect in the models where electric field considered uniform in the absorber layer.

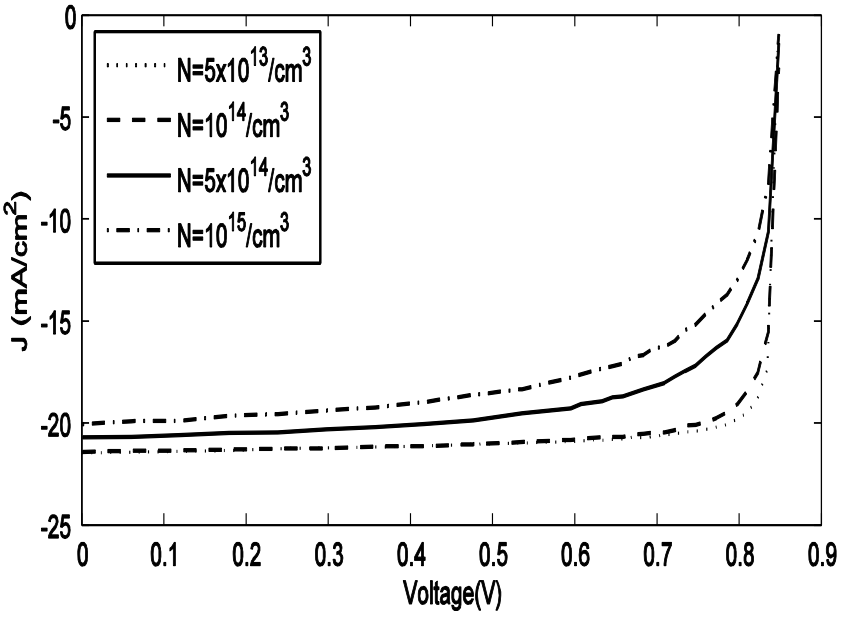

Figure 4-6: Drift current density versus voltage for different space charge density (N)

Figure 4-7 shows diffusion current density versus voltage for different space charge density. For low doped absorber layer when electric field exists everywhere in the absorber layer and diffusion current is negligible as no part of the absorber layer is without the influence of the electric field. For highly doped absorber layer, the diffusion current increases slightly with increasing space charge density at a particular voltage.

With the increase of space charge density, the depleted region width decreases and the zero electric field region width increases. In zero electric filed region, all photo generated carriers flow due to diffusion and hence it increases with space charge density.

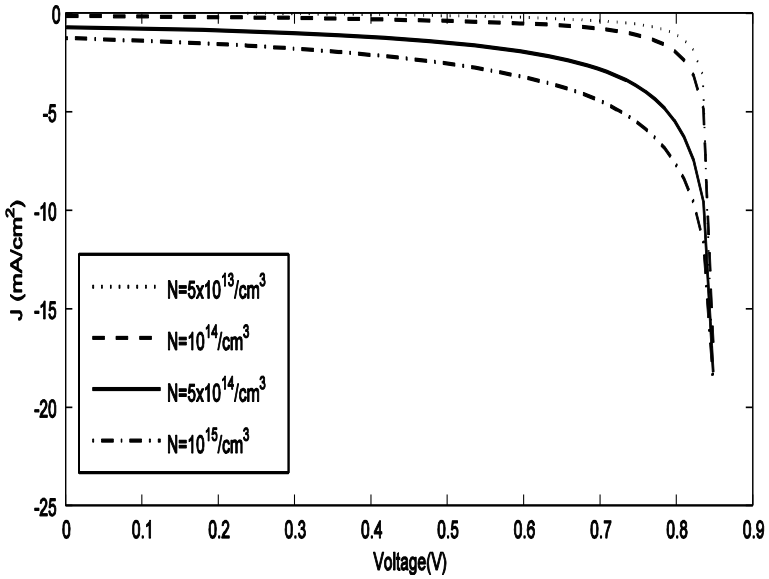

Figure 4-7: Diffusion current density versus voltage for different space charge density(N)

4.5 J/V Characteristics of CdTe Solar Cells

In our model we calculated photo current considering actual solar spectrum and practical absorption coefficient of thin film materials at different photon wavelength. The absorption coefficients for CdTe and CdS are obtained from the absorption curves in Ref. [43]. Absorption coefficients of polycrystalline CdTe and CdS as a function of photon wavelength are shown in Figure 4-8. The CdS layer significantly absorbs photons up to 500 nm of wavelength, and thus can reduce the photo current and its overall efficiency.

The CdTe layer can effectively absorbs photons up to 800 nm of wavelength, where the absortion coefficients is higher than 2×10^4 cm^{-1} and the corresponding absorption depth is 0.5 μm. Therefore, the CdTe layer thickness of 1.0 μm can effectively absorbs photons up to 900 nm of wavelength.

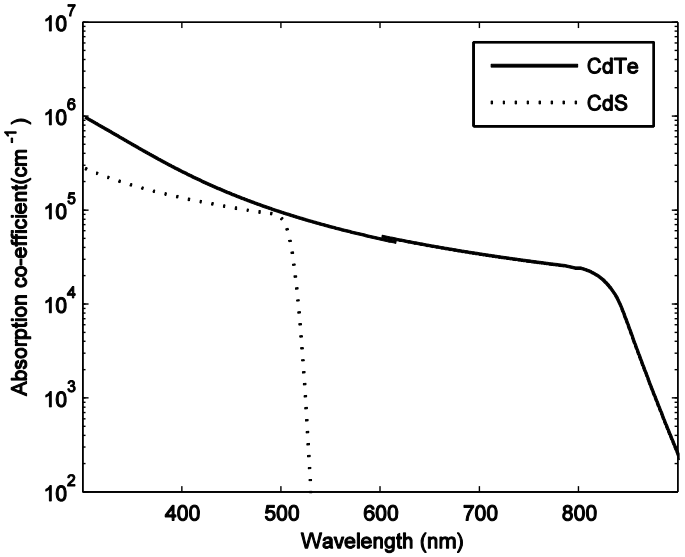

Figure 4-8: CdTe and CdS Absorption coefficients variation with wavelength.

Figure 4-9 shows the *J-V* curves of a CdS/CdTe solar cell in actual solar spectrum. The solid lines represent the proposed model considering the space charge effects [35]. The net photocurrent at any output voltage is calculated by deducting the corresponding dark current from the summation of drift and diffusion current. The dash line represents the analytical model considering uniform electric field [44]. The symbols represent experimental data of J-V characteristics and the data was taken from Fig. 6 of Ref [45]. The analytical model ignored the space charge effects and based on the assumption of uniform electric field throughout the absorber layer. In this analytical model, for all

space charge densities photo current is considered flow due to drift only. This is valid only at low space charge density. At high space charge density the zero electric field regions exists in the absorber layer and the diffusion mechanism should be considered in the zero electric field region. Therefore, in the case of high space charge density total photocurrent will be the summation of drift current and diffusion current and this fact is not addressed in the analytical model.

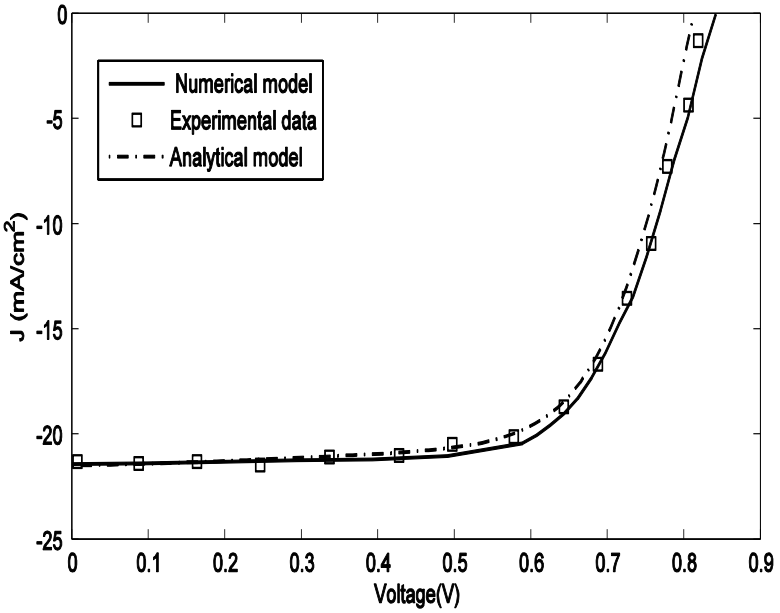

Figure 4-9: Current-voltage characteristics of a CdTe solar cell. Solid line represent proposed model, the symbol represent experimental data that were extracted from Ref [45], and the dash-dot line represent analytical model.

In our proposed model the data was taken for a CdS/CdTe thin-film solar cell and the device fabricated by vapor transport (VT) method. A typical space charge density N=2 $\times$10^14 cm^{-3} is considered for CdS/CdTe Solar cell. The CdTe thickness is 3.5 μm. The CdS thickness is 0.1 μm. The theoretical model shows a very good agreement with the

experimental data. The assumed value $\mu\tau$ for holes and electrons are $\mu_h\tau_h = 4\times10^{-6}$ cm^2/V and $\mu_e\tau_e = 1.8\times10^{-5}$ cm^2/V, which are consistent with the $\mu\tau$ values for CdTe [46,47]. Assuming typical values for electrodeposited CdTe layer, μ_h = 20 cm^2/V-s and μ_e = 180 cm^2/V-s [43] the carrier lifetimes become, τ_h= 0.2 μs and τ_e = 0.1 μs. The best fit series resistance is Rs= 4 ohm which is also in the typical range of 3~ 5 ohm in CdTe solar cell. A similar fitting was obtained by the previous model voltage dependent collection efficiency model (model 3) [45] using maximum photocurrent with complete charge collection, reverse saturation current and an effective attenuation coefficient for the whole solar spectrum as additional fitting parameters. Moreover, it also failed to distinguish the electron and hole transport properties.

4.6 Theoretical Analysis of the Proposed Model

Here we will analyze how the net photo current are affected by space charge density, transport properties of carriers, series resistance, surface recombination velocity, temperature, absorber layer width and window layer thickness. Our model realistically considers the impact of these parameters impact on the J-V characteristics.

4.6.1 Effect of Space Charge Density

Figure 4-10 shows the J/V characteristics for different space charge density. Net photo current is calculated considering drift current, diffusion current and dark current. The drift current decreases with the increase of space charge density and the diffusion current

increases with the increase of space charge density. It is clear from the figure that when space charge density is not so high short circuit current do not change significantly. This is due to the fact that in that range of space charge density depleted region width is sufficient enough to drift most of the photo generated carrier at the top edge of absorber layer. On the other hand when space charge density is sufficiently high the depleted region reduced severely and majority of the photo generated carriers are not drive by the electric field rather flow due to diffusion. Diffusion process is slower compared to drift and net current at low output voltage is decrease with the increase of space charge density. At high output voltage of the solar cell, the drift and diffusion current do not change significantly and hence total current do not change with space charge density.

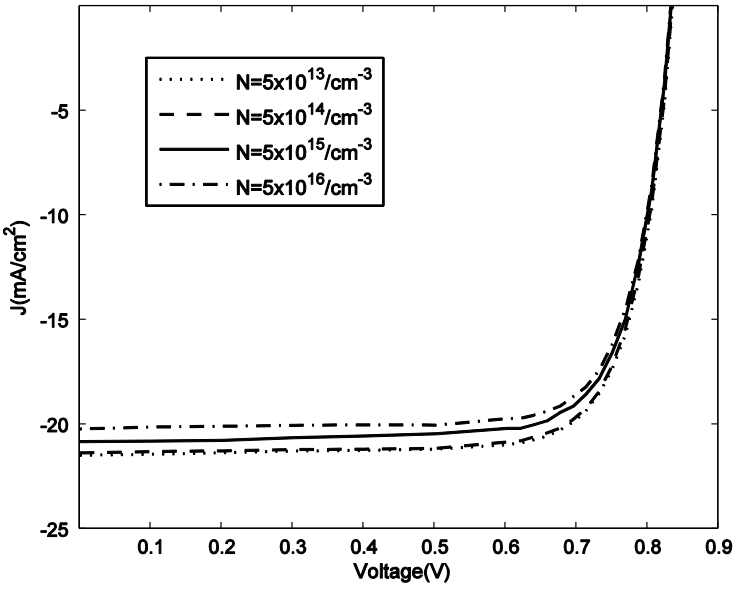

Figure 4-10: Variation of net current density with voltage for various space charge density(N) of a CdTe solar cell

4.6.2 Effect of Carrier Transport Properties

The EHPs are generated exponentially across the CdTe layer. Since the photon absorption coefficient up to 900 nm of wavelength is very high, the EHPs are mainly generated near the *n-p* interface in the CdTe layer. Therefore, electrons quickly move towards the top electrode and holes have to move a much longer distance towards the bottom electrode. Thus, the drift charge collection should mainly controlled by the hole transport properties [48]. Figure 4-11 show the *J-V* characteristics of CdS/CdTe solar cells for various levels of $\mu\tau$' products of holes. So short circuit current is affected by the hole transport properties. As dark current changed with hole properties the open circuit voltage is also changed by hole transport properties.

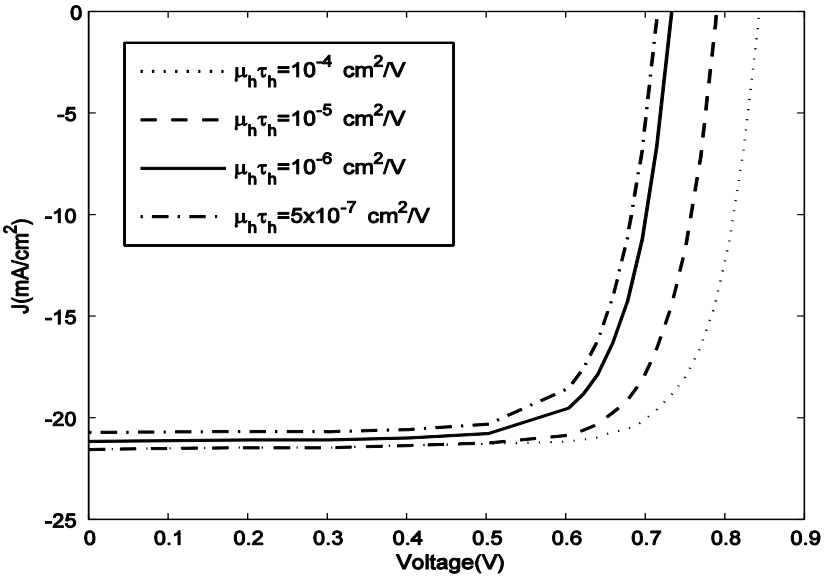

Figure 4-11: Theoretical net current density versus voltage for various level of mobility lifetime ($\mu\tau$) products of holes in CdTe solar cell

The theoretical overall efficiency varies from 11.13 % to 14.05 % by changing the $\mu_h \tau_h$ values from 5×10^{-7} cm^2/V to 10^{-4} cm^2/V. The table 4-1 shows cell efficiency for various values of $\mu_h \tau_h$.

Table 4-1: CdS/CdTe Solar cell efficiency as a function of hole carrier range.

$\mu_h \tau'_h$.(cm^2/V)	5×10^{-7}	1×10^{-6}	1×10^{-5}	1×10^{-4}
Efficiency (%)	11.13	11.72	12.94	14.05

Figure 4-12 show the *J-V* characteristics of CdS/CdTe solar cells for various levels of $\mu\tau$ products of electrons. At low output voltage the absorber layer is fully depleted, and the photo generated electrons in the n-p interface move quickly towards the top electrode. As drifted electron travel a very short distance and not affected by $\mu\tau$ products and hence short circuit current is not changed. On the other hand dark current changed with electron transport properties and hence the open circuit voltage is changed.

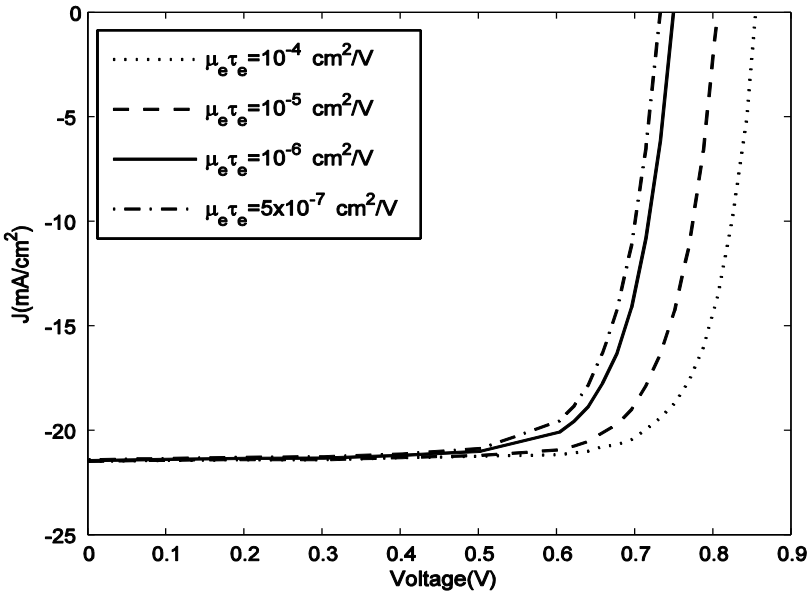

Figure 4-12: Theoretical net current density versus voltage for various levels of mobility lifetime ($\mu\tau$) products of electrons in CdTe Solar cells

The theoretical overall efficiency varies from 11.76 % to 14.24 % by changing the $\mu_e\tau_e$ values from 5×10^{-7} cm^2/V to 10^{-4} cm^2/V. The table 4-2 shows cell efficiency for various values of $\mu_e\tau_e$.

Table 4-2 : CdS/CdTe Solar cell efficiency as a function of electron carrier range.

$\mu_e\tau_e$.(cm^2/V)	5×10^{-7}	1×10^{-6}	1×10^{-5}	1×10^{-4}
Efficiency (%)	11.76	12.13	13.28	14.24

4.6.3 Effect of Series Resistance

For ideal solar cell we can assume series resistance R_S=0. For practical solar cell there must have some series resistance. The value of series resistance depends upon the materials and deposition technique. In our model we incorporate the effect of series resistance on J-V characteristics and series resistance is used as fitting parameters.. Figure 4-13 shows how J-V curve changes for different values of R_S. Series resistance do not affect the open circuit voltage. However the current near the open circuit voltage region decrease significantly with the increase of series resistance. The model demonstrated the impact of series resistance successfully which comply with the theoretical explanation of the effects of series resistance.

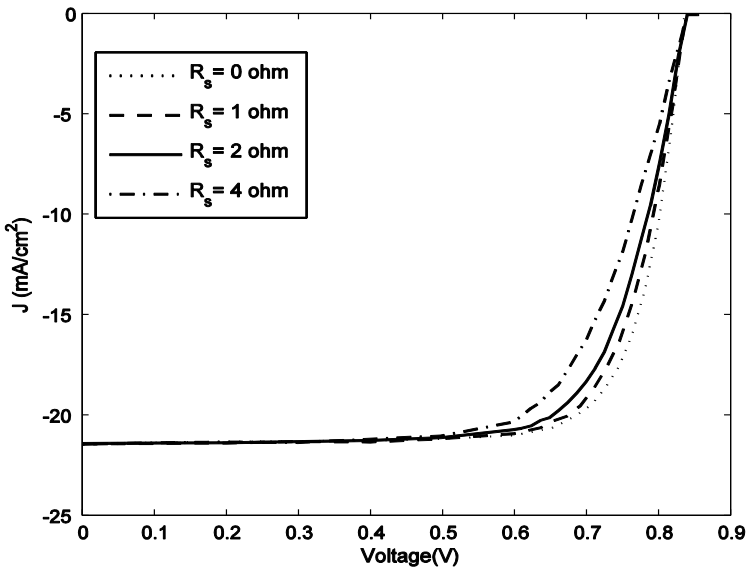

Figure 4-13: Theoretical net current density versus voltage for different series resistance (R_S) in CdTe solar cell

4.6.4 Effect of Surface Recombination Velocity

Surface recombination velocity affects the diffusion carrier distribution in the zero electric field regions of the absorber layer. With the increase of surface recombination velocity the electron concentration at the bottom edge decrease and less carrier are available to flow current. Therefore with the increase of surface recombination velocity the current J_{SC} decreases as shown in Figure 4-14.

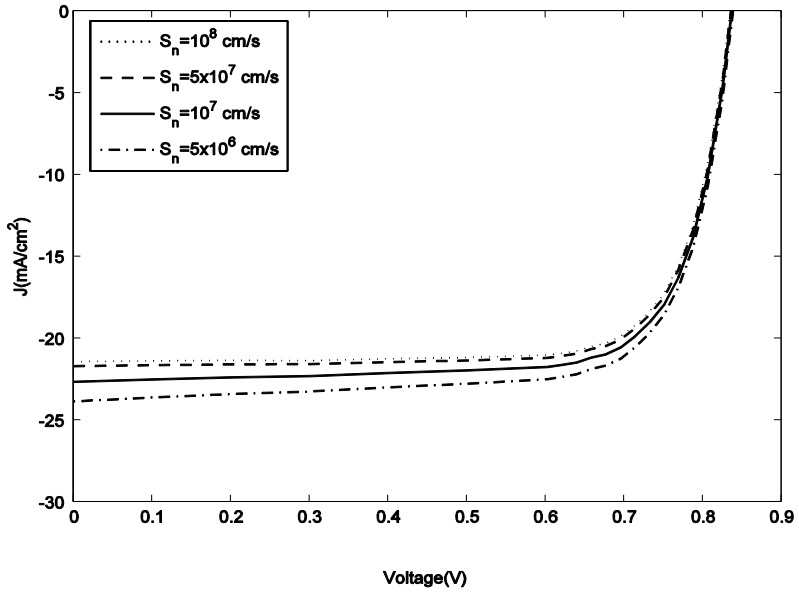

Figure 4-14: Theoretical net current density versus voltage for different surface recombination velocity (S_n) of CdTe Solar cell

The change in net current is more notably at the lower output voltage region because at low output voltage the zero electric field region width is small and electron distribution change significantly with surface recombination velocity and hence changes the current.

On the other hand at high terminal voltage the zero electric field region width is high and electron distribution does not change considerably with surface recombination velocity and the current is not changed at that voltage.

4.6.5 Effect of Temperature

Figure 4-15 shows the variation of net photocurrent with temperature. As the temperature is increased the equilibrium concentration of electrons n_i increases exponentially and so does the dark saturation current density. The increased dark current reduces V_{OC}. Therefore with the increased of temperature the efficiency of solar cell is reduced due to decrease of open circuit voltage.

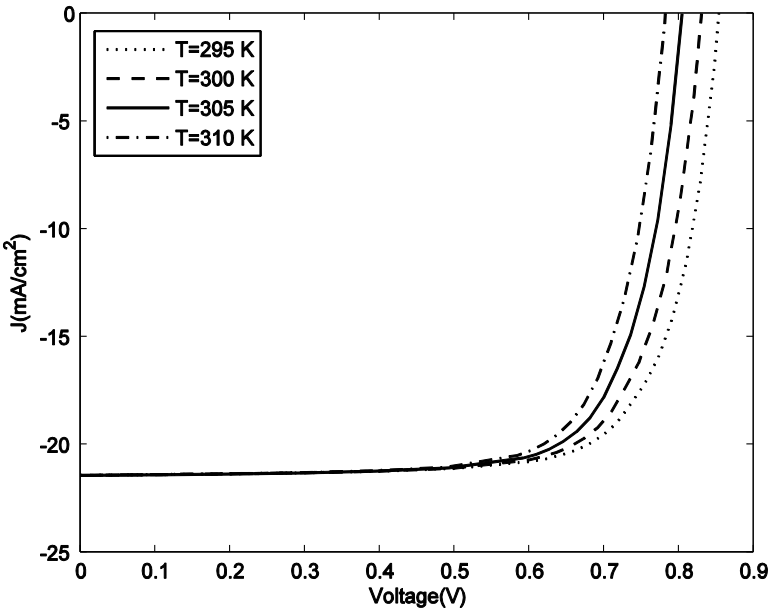

Figure 4-15: Theoretical net current density versus voltage for different temperature (T) of CdTe Solar cell

In practice increased temperature reduces the band gap and the short current is increased slightly since lower energy photons can now be absorbed. The slight increase of J_{SC} with temperature due to energy band reduction is not reflecting in our simulation because the data of the absorption co-efficient variation with temperature or energy bandgap is not available. However for all practical solar cells the net effect of increasing temperature is a reduction of efficiency because the loss of V_{OC} outweighs the gain in J_{SC}.

4.6.6 Effect of Absorber Layer Width

Figure 4-16 shows the J/V characteristics with varying the device thickness. In thin film solar cell dark current is strongly depend on recombination component compared to the diffusion component. Due to recombination, dark saturation current density linearly depends on device thickness. Therefore, the dark current increases with the increase of absorber layer thickness which reduces open circuit voltage V_{OC}.

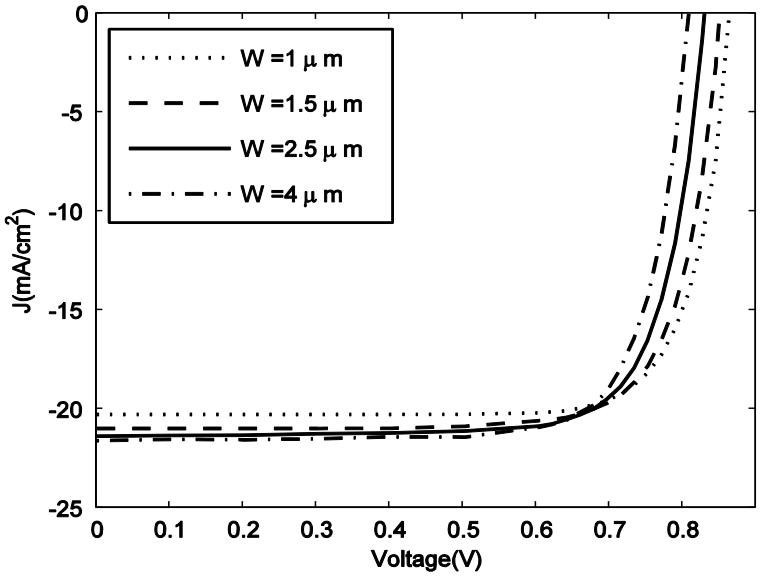

Figure 4-16: Theoretical net current density versus voltage for different absorber layer width (W) of CdTe Solar cell

On the other hand, with the increase of device length short circuit current J_{SC} is increased due to more absorption of photon. The increase of J_{SC} with the increase of device length is significant when thickness vary in the lower range ($\approx 2\,\mu m$).Beyond this thickness the J_{SC} is not increased considerably as most photons are absorbed within 2 μm. Table 4-3 shows how the efficiency of a thin film solar cell varies with device thickness. With the increase of device thickness the efficiency increases and after reaching to a maximum value, the efficiency decreases with the increase of device thickness because of trapping. Carrier loss due to trapping increases with the increase of device thickness. The proposed model can be used effectively to find the optimum thickness of absorber layer in a thin film solar cell.

Table 4-3 : CdS/CdTe Solar cell efficiency as a function of absorber layer thickness

Absorber layer thickness (μm)	1	1.5	2.5	4
Efficiency (%)	13.71	13.76	13.54	13.37

4.6.7 Effect of CdS Window Layer Thickness

As the top window layer is very thin, its effect on *J-V* characteristics is ignored in previous models. The CdS layer thickness may vary from 0.1 μm to 0.3 μm in CdTe solar cells [49]. The effect of CdS layer thickness on the incident sun spectra at CdTe layer is shown in Figure 4-17. Even 0.1 μm thick CdS layer significantly absorbs photons up to 500 nm of wavelength, and thus can reduce the photo current and its overall efficiency.

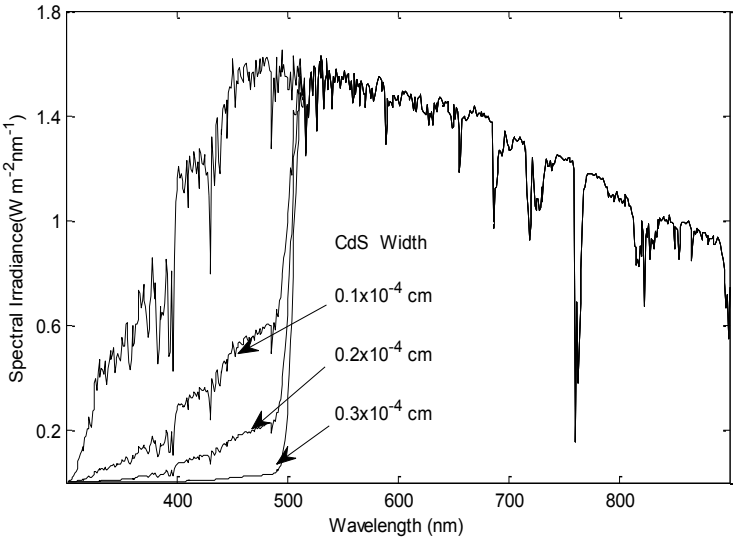

Figure 4-17: The effect of CdS layer thickness on the incident sun spectra at the CdTe layer.

Figure 4-18 shows how J-V characteristics of a CdTe solar cell change with window layer thickness. With the increase of window layer thickness, the available photon in CdTe layer decreases which reduces the current . Figure 4-19 shows the eefficiency variation of a CdS/CdTe solar cell as a function of the CdS thickness.

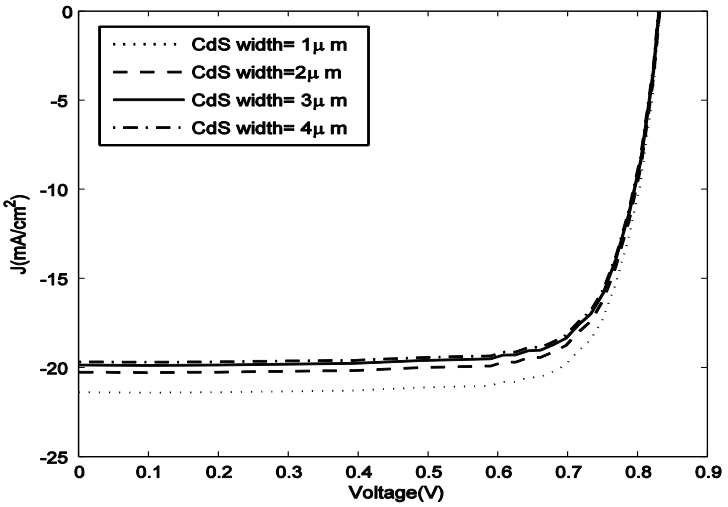

Figure 4-18: Theoretical net Net current density versus voltage for different window (CdS) layer thickness of CdTe Solar cell

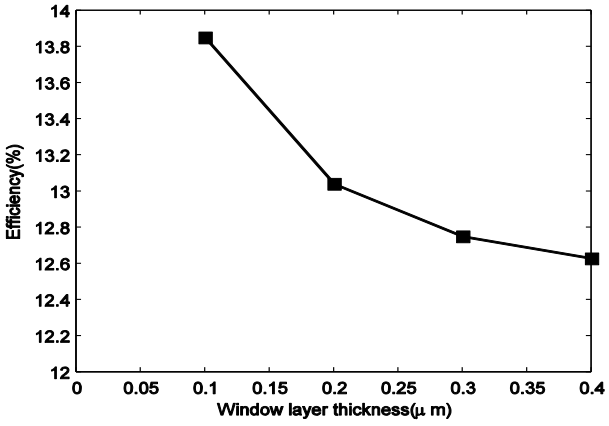

Figure 4-19: Efficiency vs. thickness of CdS layer graph of a CdTe solar cell

4.7 J/V Characteristics of CIGS Solar Cells by Proposed Model

Substrate device structured CIGS thin-film solar cell is composed of glass/Mo/Cu(InGa)Se_2 /CdS/ZnO/grid. The Cu(InGa)Se_2 layers deposited by elemental thermal evaporation and their bandgap could be varied from 1.0 to 1.7 eV by varying Ga/(In+Ga). We test our model with GIGS solar cells. The absorption coefficient for CIGS is obtained from the absorption curves in Ref. [50]. The absorption coefficient for CIGS as a function of photon wavelength is shown in Figure 4-20. Figure 4-21 shows the *J-V* curves of a GIGS solar cell at 100 % sun intensity. The symbols represent experimental data and the solid lines represent the theoretical fit to the experimental data. The experimental data were extracted from Fig.7 of Ref. [10]. The CIGS thickness is 2 μm. The CdS thickness is assumed as 0.1 μm. The theoretical model shows a very good agreement with the experimental data. Assumed value of the various parameters are $\mu_h \tau_h = 3 \times 10^{-6}$ cm^2/V and $\mu_e \tau_e = 5 \times 10^{-6}$ cm^2/V, $V_0 = 0.64$ V, $A = 1.50$ and $R = 0.25$ which are typical for CIGS devices. The best fit series resistance is Rs = 0 Ω-cm^2 , which is also reasonable for CIGS solar cell. The overall efficiency is 15.34%. The short circuit current density is 31.8 mA/cm^2 and the shape of the *J-V* curve is almost rectangular, which indicates that the carrier transport properties in CIGS are very good. The CIGS material can efficiently absorbs the incident photons up to 1200 nm of wavelength, which gives high short circuit current and high overall efficiency.

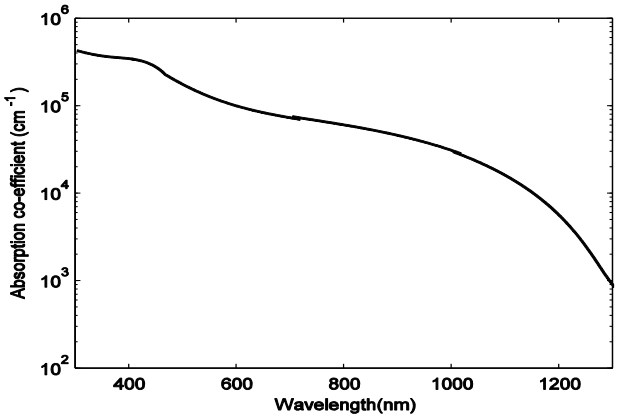

Figure 4-20: CIGS Absorption coefficients variation with wavelength.

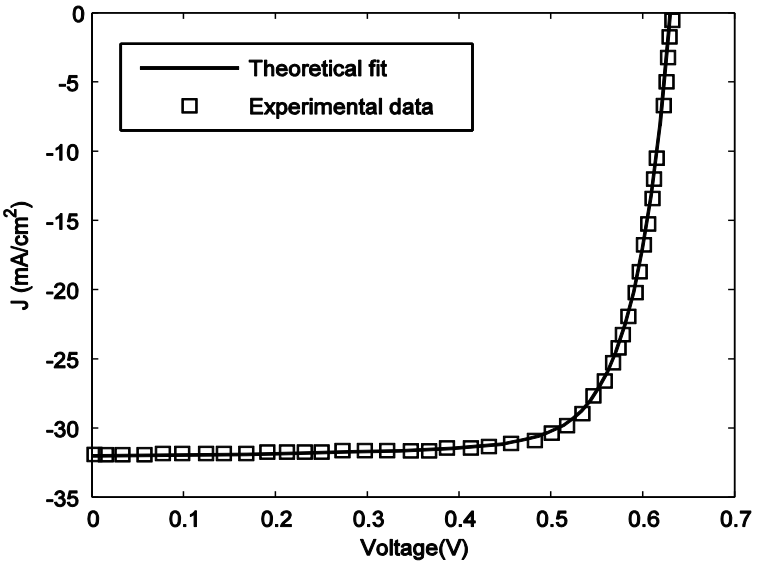

Figure 4-21: Current-voltage of a CIGS solar cell. The symbols represent experimental data and the solid lines represent the theoretical fit to the experimental data. The experimental data were extracted from Ref [10].

4.8 Summary

In this chapter, we analyze the *J-V* characteristics of various thin film solar cells with varying space charge density, carrier transport properties and operating conditions. We validate the proposed model with published experimental data on various thin film solar cells. Practical solar spectrum is used in the simulation which is more close to the physical process that occurs in the solar cell. The ideal diode current in thin film solar cells is mostly due to recombination in the depletion region. The CdTe solar cell efficiency highly depends on the carrier transport properties, temperature, and window layer thickness. The photon absorption capability over a wide spectrum is very important for achieving higher efficiency. The model shows a very good agreement with the published experimental data on various thin film solar cells.

CHAPTER 5 : CONCLUSION, CONTRIBUTIONS AND FUTURE WORK

5.1 Conclusion

We have to depend on current-voltage characteristic curve of solar cell to learn about four basic photovoltaic parameters: the efficiency, short circuit current density, open circuit voltage and the fill factor. In this thesis a model is proposed to describe the J-V characteristics of a thin film solar cell. The model considers the effect of non uniform electric filed on carrier transport. It is considered that the non uniformity of electric field depends on the space or trapped charge density in the absorber layer. The model explain how the variation of parameters such as, space charge density, series resistance, electron and hole different carrier transport properties, temperature, absorber layer width, window layer thickness, affects the J-V characteristic curve of a thin film solar cell. In this thesis the continuity equation for both electrons and holes are solved numerically considering non uniform electric field, actual solar spectrum, exponential photon absorption, exponential electron-hole pair generation across absorber layer, carrier trapping and carrier drifting in the absorber layer. Voltage dependent photo current is calculated by adding drift current in the depleted region and diffusion current in zero electric field region of the absorber layer. The overall load current is calculated considering the effect of voltage dependent forward dark current

The recombination current in the depletion region dominates over the ideal diode current in CdTe solar cells. The CdTe solar cell efficiency greatly depends on the carrier

transport properties, temperature, and window layer thickness.. The photon absorption capability over a wide spectrum and good carrier transport properties of the absorber layer are equally important for achieving higher efficiency. The model shows a very good agreement with the published experimental data on various thin film solar cells.

5.2 Contribution

A numerical model is developed to describe J/V characteristics of the $n^{+}p$ structured thin film solar cell. The effect of space charge is first shown in this thesis. When space or trapped charge density exceeds a limit, the electric field collapses and photo generated carriers outside the depleted region of the absorber layer are flow due to diffusion. This fact is considered in our model. The contributions of this thesis work are as follows:

- A numerical model is developed to study the current-voltage characteristics of thin film solar cells incorporating space charge effects.
- Carrier transport mechanisms are proposed if the electric field collapses somewhere in the absorber layer of a thin film solar cell.
- The models for calculating drift current in the depleted region and the diffusion current in the zero electric field region are proposed.
- Effects of space charge density, carrier transport properties, surface recombination velocity, series resistance, temperature, absorber layer width and window layer thickness on the J/V characteristics of thin film solar cell at different output voltage are described.

- Proposed thin film model is validated by comparing the calculated results with the recently published experimental data for polycrystalline CdTe and $CuIn_{1-x}Ga_xSe$ (CIGS).

5.2 Suggestions for Future Work

We verified the n^+p structured thin film solar cell model for the CdS/CdTe and CIGS solar cell. There are other photo sensitive materials available which have a good prospect to use as cell material. By changing the parameters in our model according to the new photoconductive material, the same model can be used to obtain the *J/V* characteristic for the corresponding solar cell. The model can be modified for a p^+n structured and verified for a-Si and other p^+n structured thin film solar cell. The model can be improved to incorporate the effect of shunt resistance on output voltage dependent photocurrent. Based on the same concept the model can be modified to describe the polycrystalline (HgI_2 , CdZnTe, poly-PbI2) X-ray detector response to exposure. The concept of drift and diffusion currents in two region of absorber layer can be applied to detector application.

REFERENCES

[1] G. W. Crabtree and N. S. Lewis, "Basic research needs for solar energy utilization" Physics Today, American Institute of Physics, Vol. 60, pp. 37-42, March 2007.

[2] Steven S. Hegedus and Antonio Luque, "Status, Trends, Challenges and The Bright Future of Solar Electricity from Photovoltaics," in Handbook of Photovoltaic Science and Engineering, Edited by A. Luque and S. Hegedus, John Wiley & Sons, 2003.

[3] Mario Pagliaro, Giovanni Palmisano, and Rosaria Criminna, "Flexible Solar Cells" Wiley-Vch,Chapter :1, pp.5, 2008.

[4] W. Hoffmann, "A Vision for PV Technology up to 2030 and beyond An industry view", ChemSusChem, vol.1, pp.880 – 891 , 2008.

[5] C. A. Wolden,J. Kurtin, J.B. Baxter,I. Repins, S. E. Shaheen, J.T. Torvik, A.A. Rockett, V. M. Fthenakis,E. S. Aydil, "Photovoltaic manufacturing: Present status, future prospects, and research needs" J. Vac. Sci. Technol. A 29(3), pp.1-16, Jun 2011

[6] http://www.tomorrowisgreener.com/worldwide-market-for-solar-panels-is-growing rapidly/ - "Worldwide market for solar panels is growing rapidly" Posted by Greener Tomorrow on February 17th, 2011

[7] http://www.wiley-vch.de/books/sample/3527323759_c01.pdf

[8] K. Yu, and J. Chen," Enhancing solar cell efficiencies through 1-d nanostructures," Nanoscale Res. Lett., vol. 4, pp.1–10, 2009.

[9] Martin A. Green, Keith Emery, Yoshihiro Hishikawa and Wilhelm Warta, "Solar cell efficiency tables (version 36)" Prog. Photovolt Appl., vol.18, pp. 346–352, 2010.

[10] S. S Hegedus, W. N Shafarman "Thin-film solar cells: device measurements and analysis" Progress in Photovoltaics Research and Applications, vol. 12, issue. 23, pp. 155-176, 2004

[11] S. S. Hegedus , "Current-Voltage Analysis of a-Si and a-SiGe Solar Cells Including Voltage-dependent Photocurrent Collection" Progress in Photovoltaics Research and Applications, vol. 5, pp.151-168 ,1997

[12] H.G. Wagemann, H. Eschrich: "Grundlagen der Photovoltaischen Energiewandlung" Teubner, Stuttgart, pp. 112, 1994

[13] K. Misiakos, F. A. Lindholm, "Analytical and numerical modeling of amorphous silicon p-i-n solar cells" J. Appl. Physics, vol.64, pp.383-393, July 1988.

[14] R. Crandall, "Modeling of thin film solar cell :uniform field approximation" J. Appl. Phys. 54, 7176 ,1983

[15] K. Taretto, U. Rau, J.H. Werner, "Closed-form expression for the current/voltage characteristics of pin solar cells" Appl. Phys. A, vol. 77, pp.865–871,2003.

[16] Hegedus S, Desai D, Thompson C., "Voltage Dependent Photo current Collection in CdTe/CdS Solar cells" Progress in Photovoltaics Research and Applications, vol.15, pp. 587–602. 2007.

[17] Palik, E.D. " Hand book of optical constants of solids, Academic Press handbook Series, Orlando, Ed., 1985

[18] P.T. Landsberg, "Recombination in Semiconductors", Cambridge University Press, 1991.

[19] W. Shockley, and W.T. Read, "Statistics of the recombination of holes and electrons", Phys. Rev. , vol.87, pp.835, 1952.

[20] A. Cuevas, G. G. Matlakowaski, P.A. Basore, C. DuBois , and R.R. king , "Extraction of the surface recombination velocity of passivated phosphorous doped silicon emitters", proc. IEEE Ist world Conference on photovoltaic Energy Conversion, Hawaii, pp. 1446-1449,1994.

[21] Meena Dadu, A. Kapoor, K.N. Tripathi, "Effect of operating current dependent series resistance on the fill factor of a solar cell," Solar Energy Materials a Solar Cells, vol. 71, pp.213–218, 2002.

[22] M. D. Archer and R. Hill, Clean Electricity from photovoltaics. Imperial College Press, 2001.

[23]T. Markvart and L. Castaner, "Practical Handbook of Photovoltaics, Fundamentals and Applications", Elsevier, 2003.

[24] G. A., "Photovoltaic materials, history, status and outlook," Materials Science and Engineering: R: Reports, vol. 40, pp. 1- 46, January 2003.

[25] P. Mints, "Analysis of Worldwide PV Markets and Five-Year Application Forecast 2009/2010", Navigant Consulting, San Francisco, CA, 2010.

[26] M. A. Green, K. Emery, Y. Hishikawa, W. Warta, "Short communication solar cell efficiency tables (version 35)", Progress in Photovoltaics: Research and Applications, vol. 18, pp. 144-150, 2010.

[27] S. O. Kasap, "Principles of electronic materials and devices," 2nd edition , McGraw-Hill, New York, 2002, chapter 1.

[28] R Sudharsanan, A Rohatgi,"Growth and process optimization of CdTe and CdZnTe polycrystalline films for high efficiency solar cells", Solar Cells, 31, 243,1991.

[29] M Eron, A Rothwarf, “Effects of a voltage-dependent light-generated current on solar cell measurements: CuInSe2/Cd(Zn)S”, Applied Physics Letters, vol.44, issue:131, 1984.

[30] S.Hegedus, “Current-voltage analysis of a-Si and a-SiGe solar cells including voltage-dependent photocurrent collection”, Progress in Photovoltaics, vol.5, issue:151, 1997.

[31] A Rothwarf, J Phillips, N Wyeth, “Junction field and recombination phenomena in the CdS/Cu2S solar cell: theory and experiment”, Proceedings of 13th IEEE Photovoltaic Specialists Conference, 399, 1978.

[32] K Mitchell, A Fahrenbruch, R Bube, “Evaluation of the CdS/CdTe heterojunction solar cell”, Journal of Applied Physics, vol.48, 4365, 1977.

[33] Liu X, sites J. “Solar-cell collection efficiency and its variation with voltage.” ,Journal of Applied physics, vol.75,577,1994

[34] R.Crandall, “Modeling of thin film solar cells: uniform field approximation”, Journal of Applied Physics, vol. 54, pp.7176-7186, 1983.

[35] **M.A.Mannan**, M.S.Anjan, M.Z.kabir,” Modelling of current-voltage characteristics of thin film solar cells” Solid State Electronics, vol. 63, pp. 49-54, 2011.

[36] M. Z. Kabir and S. O. Kasap, “Modulation transfer function of photoconductive x-ray image detectors: effects of charge carrier trapping,” J. Phys. D: Appl. Phys., vol. 36, pp. 2352-2358, 2003.

[37] M. Z. Kabir and S. O. Kasap, “Charge transport and trapping-limited sensitivity and resolution of pixellated x-ray image detectors,” Proc. SPIE – Int. Soc. Opt. Eng., 5030, pp.26-38, 2003.

[38] S.M. Sze, “Physics of Semiconductor Devices”,2nd ed., Wiley, New York, 1981, Chapter 14, pp. 802-803.

[39] D.A. Nramen, “Semiconductor Physics and Devices”,3rd ed., Mc-Graw Hill, 2003 Chapter 8, pp. 278, 302-304.

[40] J. Nelson, “The physics of solar cells”, Imperial College Press, 2003, chapter 8.

[41] C.-T. Sah, R. N. Noyce and W. Shockley, Proc. Inst. Radio Engrs. 45, 1228 ,1957.

[42] NREL (http://rredc.nrel.gov/solar/spectra/am1.5/ASTMG173/ASTMG173.html)

[43] J. Poortmans and V. Arkhipov (eds.), Thin film Solar Cells: Fabrication, Characterization and applications ,Wiley & Sons, England, 2006, Chapter 7.

[44] M. S. Anjan and M. Z. Kabir, “Modeling of current-voltage characteristics of CdS/CdTe solar cells,” Physica Status Solidi A, vol.208, no.8, pp.813-816, 2011.

[45] Steven Hegedus, Darshini Desai and Chris Thompson, “Voltage dependent photocurrent collection in CdTe/CdS solar cells”, Prog.Photovolt: Res. Appl., vol.15, pp. 587-602, 2007.

[46] M. Miyake, K. Murase, T. Hirato, Y. Awakura, “Hall effect measurements on CdTe layers electrodeposited from acidic aqueous electrolyte” J. Electroanalytical Chem, 562, 247, 2004.

[47] W.K. Metzger, D. Albin, D. Levi, P. Sheldon, X. Li, B. M. Keyes, and R. K. Ahrenkiel, “Time-resolved photoluminescence studies of CdTe solar cells” J.Appl. Phys., 94, 3549, 2003.

[48] M. Z. Kabir and S. O. Kasap, “Charge collection and absorption-limited sensitivity of X-ray photoconductors: Applications to a-Se and HgI2” Appl. Phys. Lett. 80, 1664, 2002.

[49] J. Poortmans and V. Arkhipov (eds.), Thin film Solar Cells: Fabrication, Characterization and applications ,Wiley & Sons, England, 2006, Chapter 7.

[50] S.-H. Hana and A. M. Hermann, "Effect of Cu deficiency on the optical properties and electronic structure of CuInSe2 and CuIn0.8Ga0.2Se2 determined by spectroscopic ellipsometry", Appl. Phys. Letts., vol.85, pp.576-578, 2004.